Supporting Information

Nb(V), Ta(V), and V(IV) Catalyst-Driven Development of Temperature-Responsive Self-Healing Materials Based on Methyl Methacrylate

Joanna Drzeżdżon[1,2], Marzena Białek[3], Stefania Zappia[4], Mattia Lopresti[5], Luca Palin[5,6], Katarzyna N. Jarzembska[7], Radosław Kamiński[7], Janusz Datta[2]*

[1] Department of Environmental Technology, Faculty of Chemistry, University of Gdańsk, Wita Stwosza 63, 80-308 Gdańsk, Poland

[2] Department of Polymer Technology, Gdańsk University of Technology, Narutowicza 11/12, 80-233 Gdańsk, Poland

[3] Department of Chemical Technology and Polymer Chemistry, Institute of Chemistry, University of Opole, Oleska 48, 45-052 Opole, Poland

[4] Istituto di Scienze e Tecnologie Chimiche "Giulio Natta" (SCITEC) of the Consiglio Nazionale delle Ricerche (National Research Council - CNR) via Alfonso Corti 12, 20133 Milano, Italy

[5] Department of Science and Technological Innovation, University of Eastern Piedmont, Viale T. Michel 11, 15121 Alessandria, Italy

[6] Nova Res s.r.l., Via D. Bello 3, 28100 Novara, Italy

[7] Faculty of Chemistry, University of Warsaw, Żwirki i Wigury 101, 02-089 Warsaw, Poland

*****Corresponding author: joanna.drzezdzon@ug.edu.pl

Experimental part

Materials

The following chemicals were employed in the ethylene polymerization and copolymerization processes: 1-octene (99%, Thermo Scientific), ethyl trichloroacetate (ETA, 97%, Aldrich), and CH_2Cl_2 (ACS, FP, pure p.a., POCh), which were dried using 4A molecular sieves. Ethylene (grade 3.5, Air Liquide) and nitrogen (Messer) were purified by passing through a column containing sodium metal supported on Al_2O_3. The hexane fraction (Stanlab) used as a solvent underwent purification through treatment with sulfuric acid, followed by neutralization with sodium hydroxide and rectification (with a boiling range of 65–78°C). To ensure dryness, it was refluxed over a sodium/benzophenone mixture in a nitrogen atmosphere and distilled before use. Additionally, Et_2AlCl (1.0 M in hexane, Sigma-Aldrich), $EtAlCl_2$ (1.0 M in hexane, Sigma-Aldrich), and argon (grade 5.0, Linde Gas) were used without further purification.

All chemicals required for the synthesis of the complexes and the copolymerizations of ethylene and methyl methacrylate were purchased from Merck, Darmstadt, Germany and were as follows: niobium(V) chloride (99%), tantalum(V) chloride (anhydrous, powder, 99.999% trace metals basis), N,N-Dimethylformamide (DMF, 99.8%) vanadyl acetylacetonate (≥98% purity), 4-phenylpyridine (≥97%), n-hexane (≥95.0 %), ethyl trichloroacetate (ETA, 97%), diethylaluminum chloride (Et_2AlCl, 25 wt. % in toluene), dichloromethane (99.8%), toluene (99.5% purity), dimethyl sulfoxide (DMSO, 99.8%), methyl methacrylate (MMA, ≥99%, stabilized).

Synthesis of the Nb(V), Ta(V) and V(IV) complexes

1 mmol of $NbCl_5$ dissolved in 10 ml of CH_2Cl_2 was mixed with 1.2 mmol of DMF. The synthesis was carried out under a nitrogen atmosphere. The solution was stirred for 40 minutes at room temperature until it became clear and changed color from yellow to orange. Then, 15 mL of n-hexane was added to precipitate the fine crystalline orange complex. The crystals were collected at 71 % yield. Anal. Calcd (%) for $C_6H_{14}N_2O_3Cl_3Nb$: C, 19.91; H, 3.87; N, 7.75. Found: C, 19.21; H, 3.67; N, 7.78. FT-IR (cm^{-1}) (see Supplementary Material): 3103 (m), 1651 (s), 1438 (m), 1332 (m), 1274 (m), 1125 (m), 802 (m), 691 (m), 695 (m). TGA: I step 71 °C (2% mass loss).

1 mmol of $TaCl_5$ dissolved in 10 ml of CH_2Cl_2 was mixed with 1 mmol of 2-phenylpyridine and 1.2 mmol of DMF. The synthesis was carried out under a nitrogen atmosphere. The solution was stirred for 40 minutes at room temperature until it became clear and turned yellow. Then, 15 mL of n-hexane was added to precipitate the fine crystalline product. The crystals were collected at 44 % yield. Anal. Calcd (%) for $C_{23}H_{22}N_2Cl_9Ta$: C, 33.40; H, 3.44; N, 3.39. Found: C, 33.54; H, 3.25; N, 3.49. FT-IR (cm^{-1}) (see Supplementary Material): 3315 (m), 3064 (s), 1645 (s), 1661 (s), 1427 (m), 1363 (m), 866 (s), 695 (m). TGA: I step 95 °C (2% mass loss).

2 mmol of $VO(acac)_2$ was dissolved in 10 mL of a methanol/water mixture (9 mL methanol and 1 mL water). Then it was mixed with 2 mmol of 4-phenylpyridine (which was also dissolved in 10 mL of methanol). The resulting mixture was heated under a reflux condenser at the boiling point of the solvent for 2 hours. After

allowing it to cool to room temperature over 2 days, dark-green crystals of the coordination compound $VO(acac)_2$(4-phenylpyridine) were obtained. The crystals were collected at 83% yield. Anal. Calcd (%) for $C_{21}H_{23}NO_5V$: C, 59.95; H, 5.47; N, 3.33. Found: C, 59.89; H, 4.93; N, 3.71. FT-IR (cm^{-1}) (see Supplementary Material): 3426 (s), 3071 (m), 3295 (m), 2452 (m), 1645 (s), 1509 (s), 1395 (m), 937 (m), 767 (m). TGA: I step 77 °C (2% mass loss).

Diffraction measurements and structural solution

Single-crystal X-ray measurements of Nb(V) and Ta(V) complexes were performed on a Rigaku Oxford Diffraction SuperNova instrument equipped with a microfocus copper X-ray source (Cu K_α radiation, λ = 1.54184 Å). During the measurement crystal was maintained at 100 K with the use of an Oxford Cryosystems nitrogen gas-flow device. Unit-cell parameter determination and raw diffraction image processing were performed with the native diffractometer *CRYSALISPRO* software suite. Structures were solved using an intrinsic phasing method as implemented in the *SHELXT* program[1] and refined with the *JANA* package[2] within the independent atom model approximation. The hydrogen atoms were placed geometrically (d_{C-H} = 0.96 Å, d_{N-H} = 0.87 Å). The riding model for the hydrogen thermal motion parameters was applied ($U^H_{iso} = 1.2 \cdot U^C_{eq}$ or $1.5 \cdot U^N_{eq}$). For more details see Supporting Information.

X-ray diffraction measurements on single crystals (SC-XRD) of V(IV) complex were performed using a Rigaku Oxford Xcalibur diffractometer equipped with a graphite-monochromated Mo-Kα radiation source (λ = 0.71073 Å). The collected data underwent data reduction and absorption corrections, which were performed using the CrysAlisPRO software (version 42.49). The crystal structure was determined via direct methods exploiting SIR2019[3] and the refinement was conducted against F^2 for all reflections employing SHELXL-2013[4]within the Olex2 interface [5]. Hydrogen atoms were added to the structure exploiting independent atom model [6]. The structure packing visualization and void calculation were performed using CCDC Mercury software [7].

Crystallization of the $VO(acac)_2$ complex frequently resulted in twinned crystals, typically consisting of 2 to 5 individual crystallites. Despite repeated attempts, a single crystal of the V(IV)-based compounds could not be obtained. Consequently, de-twinning of the SC-XRD data was essential for resolving the structure. The analyzed sample contained two crystallites, with a total crystal size of approximately 50 μm. The data from each crystallite were separated into distinct datasets, and the structure was refined using the dataset with the highest number of reflections. Although the completeness of this dataset was 89%, likely due to peak overlap from the twin domains, the refinement yielded highly satisfactory agreement indices (Table S2, even in the presence of some missing reflections).

The original CIF files of all Nb(V), Ta(V) and VO(IV) complexes are also available from the Supporting Information, or can be retrieved from the Cambridge Structural Database (CSD) [8] (deposition numbers: CCDC 2391112, 2391113, 2383525).

First principle calculation

Geometric optimization of the V(IV) complex compound was performed using GAUSSIAN software (ver. 16)[9] exploiting the B3LYP functional (as evidenced by the XRD analysis). LANL2DZ pseudopotential was then chosen for its reliability in modeling transition-metal complexes. The initial molecular model was derived from the molecular structure obtained via SC-XRD (Model 1). For comparison, and to explore the conformational flexibility of the complex, in order to find the minimal energy torsional conformation of the bipyridyl system, a model consistent with Figure 2 (in the manuscript file) by Caira et al. was also used (Model 2). Key geometric parameters, including bond lengths, angles, and ligand orientations, are summarized in Table S4.

Physico-chemical testing methodology for complex compounds

Elemental analysis of the complex compounds was performed using the Elementar Vario EL III analyzer (CARBO ERBA type CHNS-O 1108). The samples, which were homogeneous and dry, weighed 2 mg. The FT-IR spectra were obtained in the range of 4500–500 cm^{-1} using a KBr pellet. A DLATGS detector (Branch Ü berlingen, Germany) was employed, and the measurements were performed with the IFS66 instrument from BRUKER (Branch Ü berlingen, Germany), which offered a resolution of 0.12 cm^{-1}. Thermogravimetric (TG) analyses were performed on samples (approx. 10 mg each) under a nitrogen atmosphere using a TG 209F3 instrument (NETZSCH, Germany). The heating rate was set to 10 K/min, with the temperature range spanning from 35 to 800 °C.

The UV-Vis diffuse reflectance spectra UV-Vis DRS were recorded using a UV-Vis spectrophotometer in the range of 200–800 nm (SHIMADZU, UV-2600).

Ethylene polymerization and ethylene/1-octene copolymerization

Ethylene polymerization was performed using a 500 mL Büchi glass autoclave equipped with the magnetic stirrer and heating-cooling jacket. Hexane (100 mL), ethyl trichloroacetate, activator and solution of the transition metal compound in CH_2Cl_2 were introduced into the preheated and nitrogen-purged reactor. Finally, ethylene was added. Each polymerization was conducted under 5 bar of ethylene at the set temperature. The ethylene pressure and reactor temperature were kept constant in the course of polymerization. Reaction was terminated by venting the reactor and transferring the obtained mixture to a dilute solution of hydrochloric acid in methanol. The polymer was filtered, washed with methanol and dried to constant weight in a vacuum oven. In the case of ethylene/1-octene copolymerization, the predetermined amount of comonomer was introduced to the reactor after the solvent.

Characterization methods of polyethylene and ethylene/1-octene copolymers

FT-IR spectra of ethylene homo- and copolymers, prepared in the form of a foil or tablet with KBr, were recorded in the range from 4000 to 400 cm^{-1} with a resolution of 2 cm^{-1} on the Nicole Nexus 2002 FTIR spectrometer. Determination of comonomer content in copolymers was made in accordance with the literature [10] using the calibration curve for ethylene/1-octene copolymers (Equation 1), where A_{CH3} is the absorbance of the band characteristic for symmetrical in-plane bending deformations of CH_3 group (1379 cm^{-1}) after separation from the influence of the band at 1368 cm^{-1} and A_{CH2} is the absorbance of the band characteristic for symmetrical in-plane bending deformations of CH_2 group (1369 cm^{-1}) after separation from the influence of the band at 1379 cm^{-1}.

$$X\ (\%mol) = 1.721 \cdot \left(\frac{A_{CH3}}{A_{CH2}}\right)^2 + 4.0123 \cdot \left(\frac{A_{CH3}}{A_{CH2}}\right) - 0.0029 \quad (1)$$

DSC analyses were performed using a DSC 1 calorimeter from Mettler Toledo at the heating rate 10°C/min. The heating-cooling-heating cycles were performed and the melting temperatures (T_m) and and melting enthalpies (ΔH) were obtained from the second heating cycle. The degree of crystallinity (X_C) was calculated assuming that the enthalpy of melting of completely crystalline polymer is equal to 290 J/g [11]. Molecular weight and molecular weight distribution (MWD) of polymers were measured by high temperature size exclusion chromatography (HT-SEC) using GPCV2000 system from Waters equipped with a differential refractometer (DRI) and set of three Shodex HT (806M-805-804) columns from Showa Denko. Polymers were dissolved in o-dichlorobenzene with addition of butylated hydroxytoluene (BHT) as antioxidant (0.05%) at 160 °C for one hour. The prepared samples with concentration of around 1 mg/ml were then analyzed at 135 °C under a flow rate of 0.8 mL/min. Sixteen narrow MWD polystyrene standards with peak molecular weight ranging from 3,280,000 g/mol to 162 g/mol (PS monomer) were used for calibration. ^1H and $^{13}C\{^1H\}$ NMR spectra of polymers and copolymers were recorded on a Bruker Avance III HD 400 MHz spectrometer at 110°C (external standard TMS for ^1H, ^{13}C) using o-dichlorobenzene-d_4 as a solvent unless stated otherwise.

Synthesis of materials based on methyl methacrylate

The process was carried out under a nitrogen atmosphere at 65°C. Initially, a solution containing 3 μmol of the V(IV) or Nb(V) or Ta(V) complex compound dissolved in a mixture of 1 mL toluene and 1 mL DMSO was prepared in a glass cell. Then, the activator Et_2AlCl was gradually added, followed by the addition of MMA, and ethylene (under 1 bar) in the next step (in addition, a synthesis was also carried out using only methyl methacrylate without introducing ethylene). The activator was added in a molar ratio to the complex compound of 1:1500. Preparation of self-healing materials based on methyl methacrylate was carried out for systems with different volumes of MMA: (1) 20 vol.% the total volume of the reaction mixture, (2) 30 vol.% the total volume of the reaction mixture, and (3) 50 vol.% the total volume of the reaction mixture. The mixture was stirred until a white gel formed. Finally, the product was drained, washed with methanol, and dried at 35°C to a constant weight.

Characterization methods of materials based on methyl methacrylate

Molecular weight and molecular weight distribution (MWD) of polymers were determined by MALDI-TOF-MS:

$$Mn = \frac{\sum\left[\left(\frac{m}{z}\right) \cdot Area\right]}{\sum Area} \quad (2)$$

$$Mw = \frac{\sum[(\frac{m}{z})^2 \cdot Area]}{\sum\left[\left(\frac{m}{z}\right) \cdot Area\right]} \quad (3)$$

The spectra were recorded using a Bruker Biflex III spectrometer with 2,5-dihydroxybenzoic acid (DHB) as the matrix. FT-IR spectra of the copolymers, prepared as KBr tablets, were recorded on a BRUKER IFS 66 spectrophotometer, covering the range from 4000 cm^{-1} to 650 cm^{-1}. FT-IR spectra of polyMMA, prepared in the form of a foil or tablet with KBr, were recorded in the range from 4000 to 400 cm^{-1} with a resolution of 2 cm^{-1} on the Nicole Nexus 2002 FTIR spectrometer. Thermogravimetric (TG) analyses were performed on samples (approx. 10 mg each) under a nitrogen atmosphere using a TG 209F3 instrument (NETZSCH, Germany). The heating rate was set to 10 K/min, with the temperature range spanning from 35 to 800 °C. Differential scanning calorimetry (DSC) analysis was performed using a DSC 204 F1 Phoenix® calorimeter (NETZSCH, Selb, Germany). Samples weighing approximately 7 mg were sealed in aluminum crucibles and subjected to two heating cycles from −80 °C to 300 °C at a scanning rate of 10 °C/min, followed by a cooling cycle from 300 °C to −80 °C at the same rate. All measurements were conducted under a nitrogen purge gas flow of 20 mL/min. Peak identification was carried out using a sigmoidal baseline. The NMR spectra were recorded on a Bruker Avance III HD 400 MHz spectrometer using $CDCl_3$ as a solvent unless stated otherwise. The morphology of the samples was analyzed using a FlexSEM 1000 from Hitachi. To improve conductivity within the vacuum chamber, the samples were coated with a thin layer of gold-palladium before observation.

Hardness Testing

The hardness of the samples was measured at room temperature using a Shore A Durometer (Zwick Roell Group, Germany) in compliance with the ISO 868 standard. The reported values represent the average of measurements taken at ten different points for each sample type.

Rheological Study

Rheological measurements were conducted using a Brookfield R/S+CPS rheometer with a cone-plate geometry (C50-2 cone). The tests were performed at temperatures of 60°C and 70°C. A fixed and

controlled shear rate was applied during the measurements, which were analyzed using Rheo3000 software version 1.2.1377.1. The following procedure was used:

- Shear rate increased from 0 to 300 s^{-1} over 120 seconds.
- Shear rate was maintained at 300 s^{-1} for 120 seconds.
- Shear rate decreased from 300 to 0 s^{-1} over 120 seconds.

Several rheological models were applied to best describe the flow behavior of the fluids. Three commonly used models were evaluated: Newton's, Herschel-Bulkley's, and Ostwald-de Waele's. These models are described below:

Herschel-Bulkley model - This model represents the flow behavior of nonlinear plastic-viscous fluids. The equation for this model is:

$$y=k_1+k_2x^{k_3} \quad (4)$$

Newton's model - Characterized by ideal fluids, it shows a linear relationship between shear stress and shear rate. The equation is:

$$y=k_2x \quad (5)$$

Ostwald-de Waele model -This model describes shear-thinning fluids that do not exhibit a yield point. The equation is:

$$y=k_2x^{k_3} \quad (6)$$

where:

x = shear rate [s^{-1}]

y = shear stress [Pa]

k_1 = yield stress [Pa]

k_2 = consistency index [-]

k_3= flow behavior index [-].

The main text of the article should appear here with headings as appropriate.

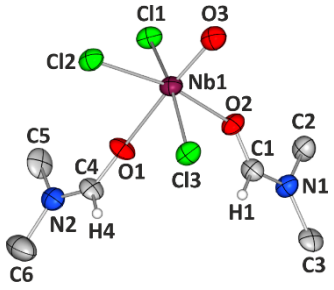

(*a*)

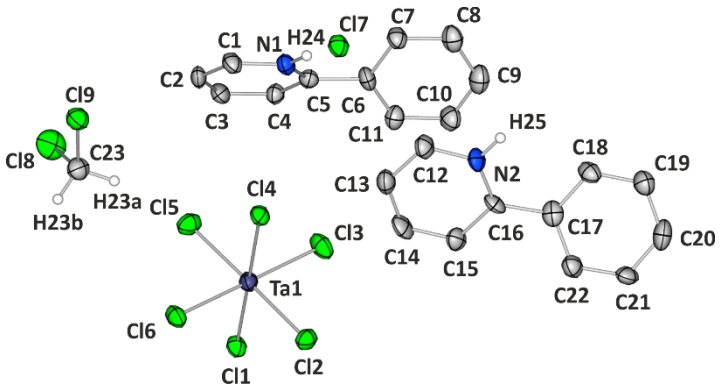

(*b*)

Figure S1. Molecular structure of the studied compounds along with the labelling scheme: (*a*) Nb(V) complex and (*b*) Ta(V) complex. Atomic thermal motion is represented as ellipsoids drawn at the 50% probability level. Some hydrogen atoms are removed for clarity.

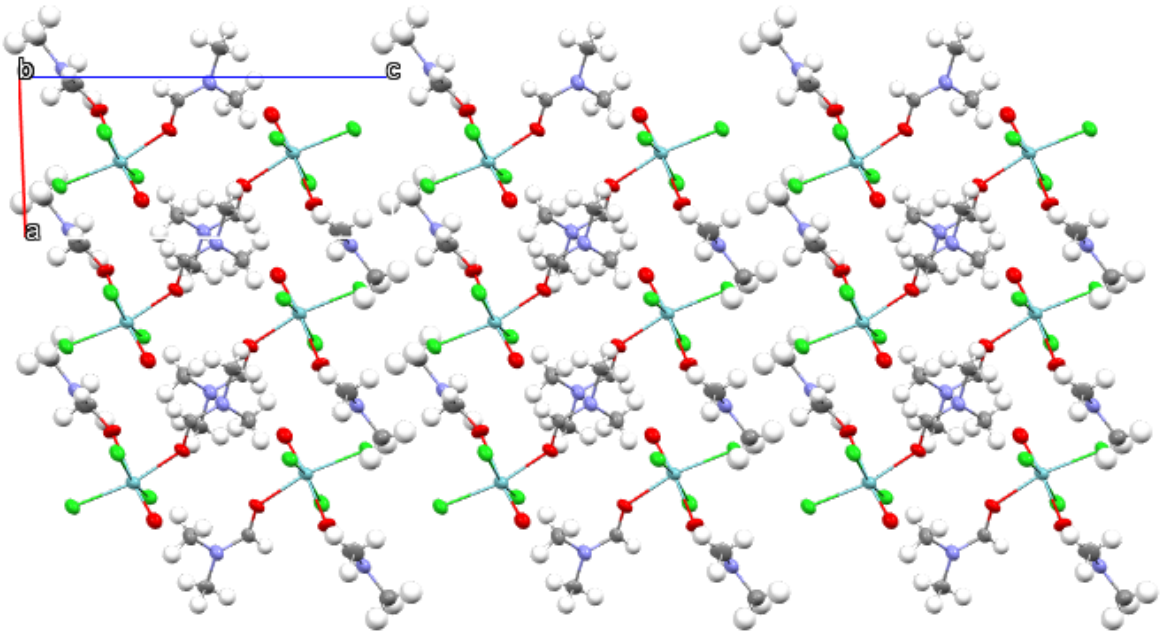

(*a*)

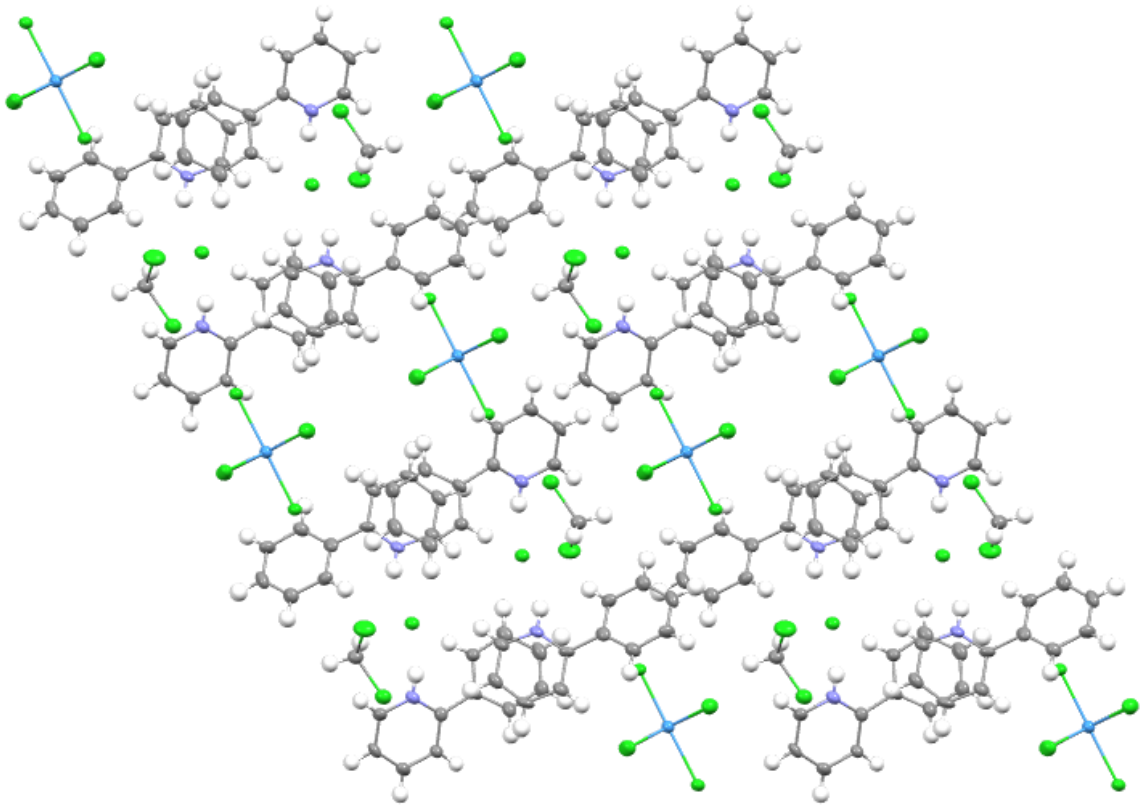

(*b*)

Figure S2. Crystal packing of the studied systems: Nb(V) complex viewed along the ^{Y} (*a*) and Ta(V) complex along the ^{X} (*b*) axes, respectively.

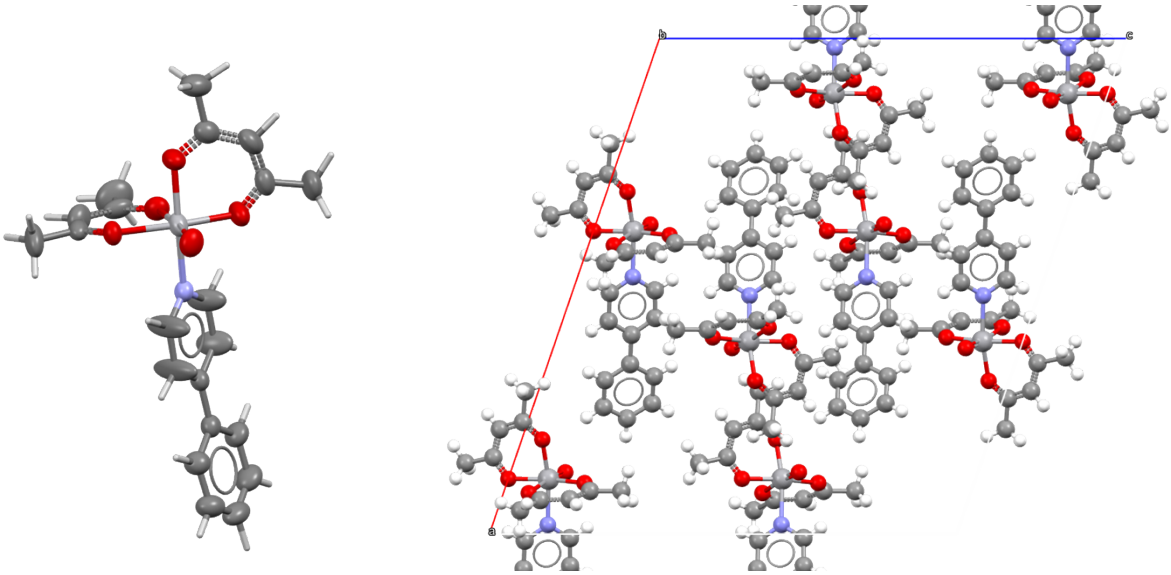

(a) *(b)*

Figure S3. Asymmetric unit (a) and packing (b) of the vanadium(IV) complex.

Table S1. Selected X-ray data collection, processing and refinement parameters for the studied multi-component crystal structure - Nb(V) and Ta(V) complexes.

Moiety formula	$NbCl_3O$ + $2(C_3H_7NO)$	$[TaCl_6]^-$ + Cl^- + $2[C_{11}H_{10}N]^+$ + CH_2Cl_2
Moiety formula mass, M_r / a.u.	361.45	826.43
Crystal system	triclinic	triclinic
Space group	$P\bar{1}$ (No. 2)	$P\bar{1}$ (No. 2)
Z	2	2
F_{000}	360	800
Crystal colour & shape	small colourless block	small colourless cut crystal
Crystal size / mm^3	0.10×0.07×0.04	0.05×0.04×0.02
T / K	100	100
a / Å	6.196(2)	7.283(2)
b / Å	8.560(2)	15.243(3)
c / Å	13.574(3)	15.412(3)
α / Å	77.68(3)	60.45(3)
β / Å	83.50(3)	88.99(3)

γ / Å	68.93(3)	86.12(3)
V / Å^3	655.8(3)	1484.8(7)
d_{calc} / g·cm^{-3}	1.8304	1.8486
θ range	3.34−76.00°	3.30−76.13°
Absorption coefficient, μ / mm^{-1}	13.061	14.425
No. of reflections collected / unique	9586 / 2695	15934 / 5995
R_{int}	5.85%	5.00%
No. of reflections with $I > 3\sigma(I)$	2257	4764
No. of parameters / restraints / constraints	136 / 0 / 56	316 / 0 / 88
$R[F]$ $(I > 3\sigma(I))$	6.35%	4.12%
$wR[F^2]$ (all data)	16.38%	12.07%
$\varrho_{res}^{min/max}$ / e·Å^{-3}	−1.67 / +2.09	−1.35 / +1.96
CCDC number	2391112	2391113

Table S2. Crystal data and structure refinement parameters for the complex compound $VO(acac)_2$(4-phenylpyridine)

Chemical formula	$C_{21}H_{23}NO_5V$
Formula weight/g·mol^{-1}	420.34
Crystal system	Monoclinic
Space group	C2/c
a/Å	24.2547(15)
b/Å	8.0765(5)
c/Å	21.6591(12)
α/°	90
β/°	108.968(7)
γ/°	90
V/Å^3	4012.5(4)
Z	8
T/K	293(2)
λ_{Mo}/Å	0.71073
ρ_{calc}/g·cm^{-3}	1.392
F(000)	1752
μ/mm^{-1}	0.526
θ range/°	2.952-25.332
Goodness of fit on F^2	1.048
Final R_1 value (I>2σ(I))	0.0708
Final wR_2 value (I>2σ(I))	0.1873
CCDC number	2383525

Table S3. Bond distances table. Bonds involving hydrogen atoms are not reported as they have been placed in their expected positions exploiting independent atom model.

Atom 1	Atom 2	Cyclicity	Length (Å)(std.dev.)
V1	O1	cyclic	1.991(3)
V1	O2	cyclic	2.136(4)
V1	O3	cyclic	1.966(3)
V1	O4	cyclic	1.978(4)
V1	O5	acyclic	1.603(4)
V1	N1	acyclic	2.155(4)
O1	C3	cyclic	1.261(6)
O2	C4	cyclic	1.255(6)
O3	C8	cyclic	1.276(6)
O4	C5	cyclic	1.247(5)
N1	C18	cyclic	1.297(8)
N1	C20	cyclic	1.283(8)
C1	C2	acyclic	1.465(6)
C1	C15	cyclic	1.337(7)
C1	C21	cyclic	1.348(9)
C2	C6	cyclic	1.394(7)
C2	C7	cyclic	1.387(8)
C3	C11	cyclic	1.355(8)
C3	C17	acyclic	1.503(8)
C4	C11	cyclic	1.388(9)
C4	C19	acyclic	1.50(1)
C5	C10	cyclic	1.391(9)
C5	C14	acyclic	1.491(9)
C6	C13	cyclic	1.378(7)
C7	C12	cyclic	1.373(7)
C8	C10	cyclic	1.383(9)
C8	C16	acyclic	1.498(7)
C9	C12	cyclic	1.360(8)
C9	C13	cyclic	1.354(9)
C15	C18	cyclic	1.373(7)
C20	C21	cyclic	1.35(1)

Table S4. Selected relevant angles from model 1 (SC-XRD), model 2 (Caira et al.) before and after geometric optimization by first principle calculations.

Angles (°)					
Atom1	**Atom2**	**Atom3**	**Model 1 (SC-XRD)**	**Model 2 (Caira *et al.*)**	**Optimized**
O3	V1	N1	167.3(2)	167.3(2)	166.7
V1	N1	C1	173.0(2)	173.0(2)	178.3
V1	N1	C9	169.4(1)	169.4(1)	178.2
C11	V1	O3	89.2(1)	89.2(1)	79.4
C10	V1	O5	93.1(2)	93.1(2)	102.3
Torsion angles (°)					
Atom1	**Atom2**	**Atom3**	**Atom4**	**Model 1 (SC-XRD)**	**Model 2 (Caira *et al.*)**	**Calculations**
O3	V1	N1	C20	-154.6(7)	115.3(8)	-152.03
O3	V1	N1	C6	177.0(5)	86.9(5)	177.76
C21	C1	C2	C6	-1.1(8)	-1.1(1)	-32.51
C11	V1	N1	C20	-91.6(5)	178.4(4)	-101.43
C10	V1	N1	C20	138.4(5)	48.4(4)	145.61
O5	V1	N1	C20	42.3(5)	47.6(4)	37.14

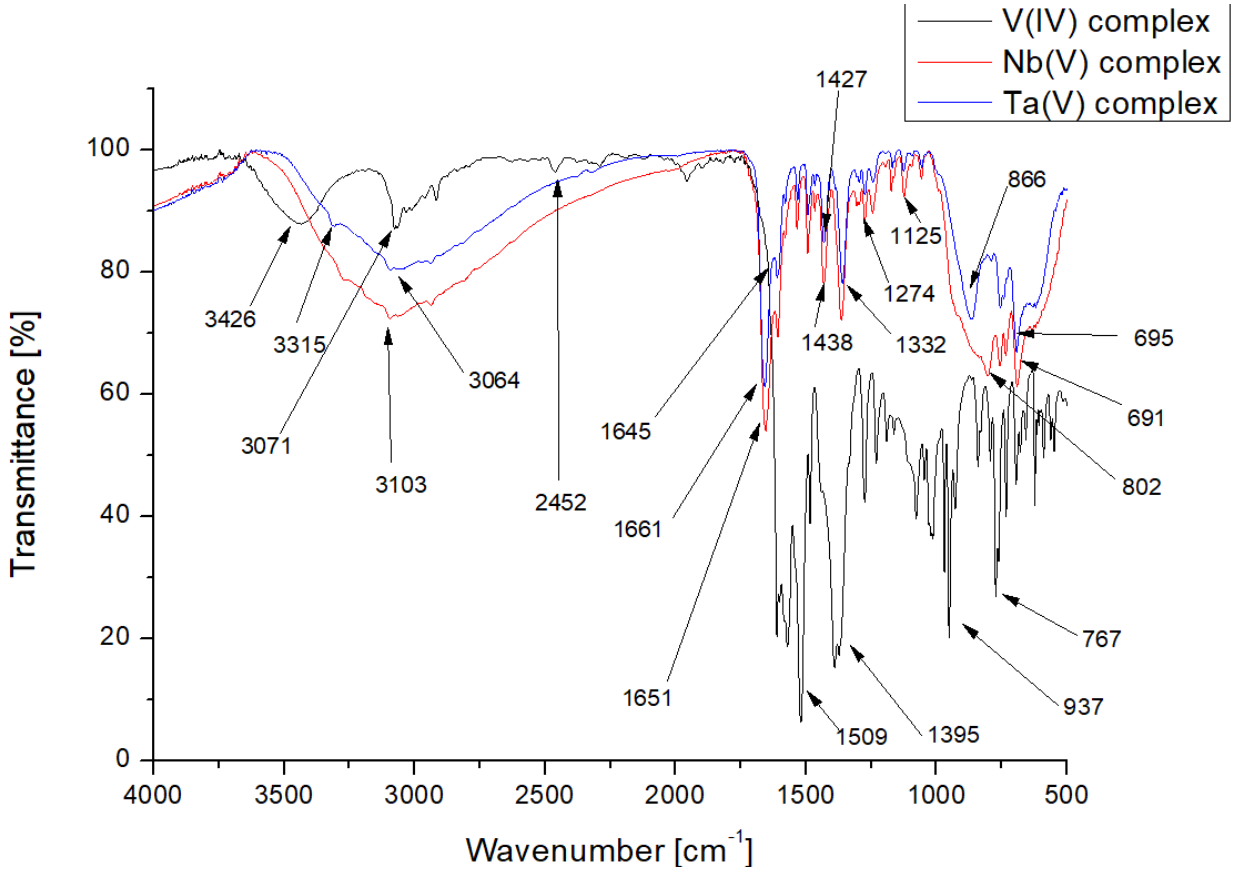

Figure S4. FTIR spectra of Nb(V), Ta(V), V(IV) complexes.

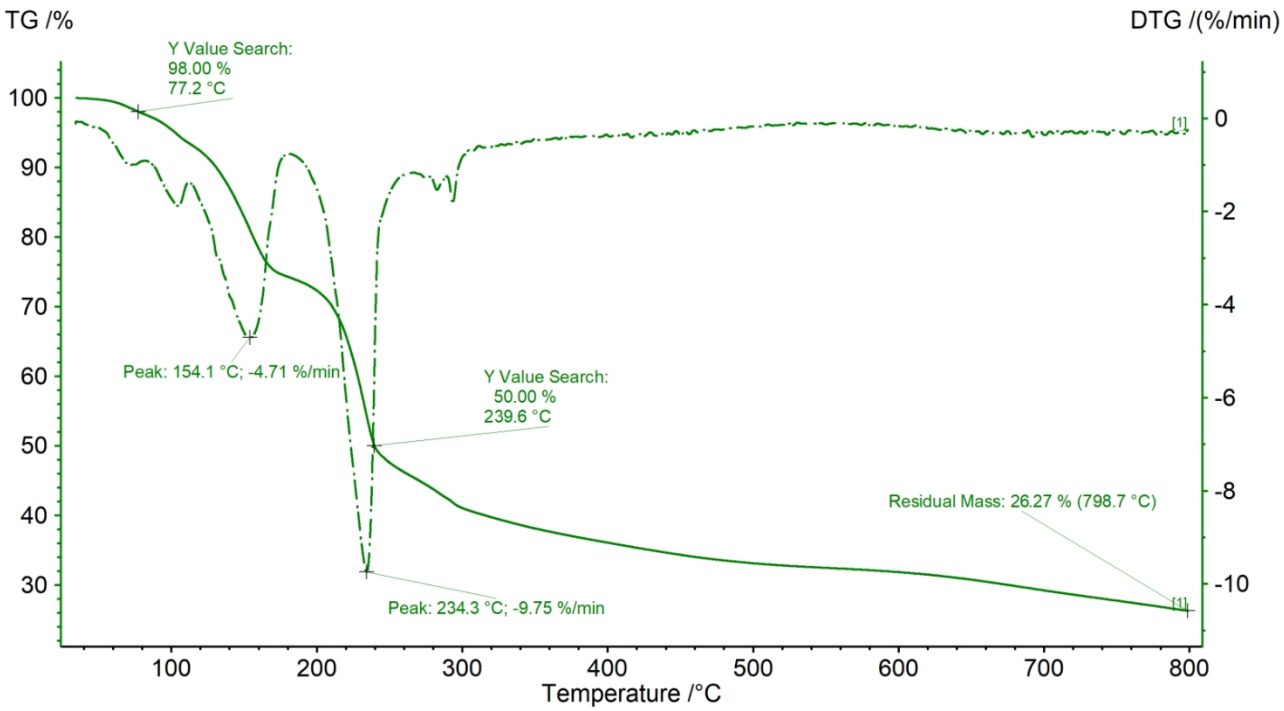

Figure S5. TG analysis of V(IV) complex – $VO(acac)_2$(4-phenylpyridine)

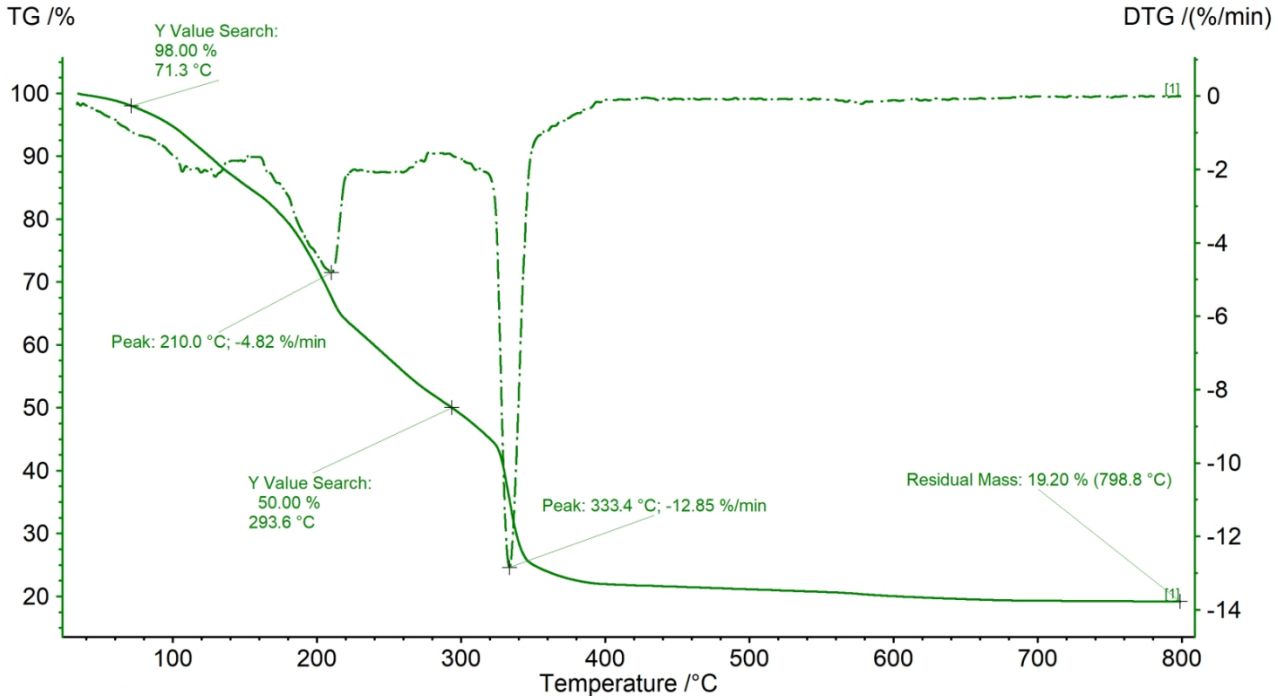

Figure S6. TG analysis of Nb(V) complex

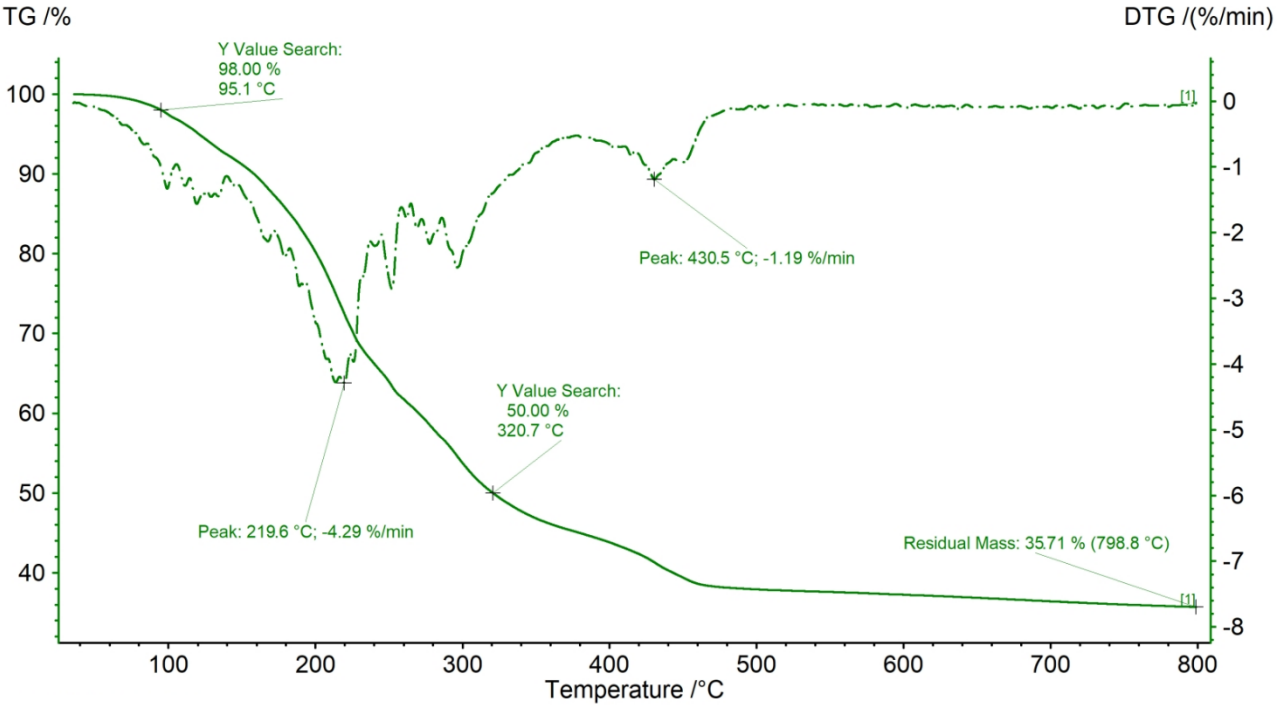

Figure S7. TG analysis of Ta(V) complex

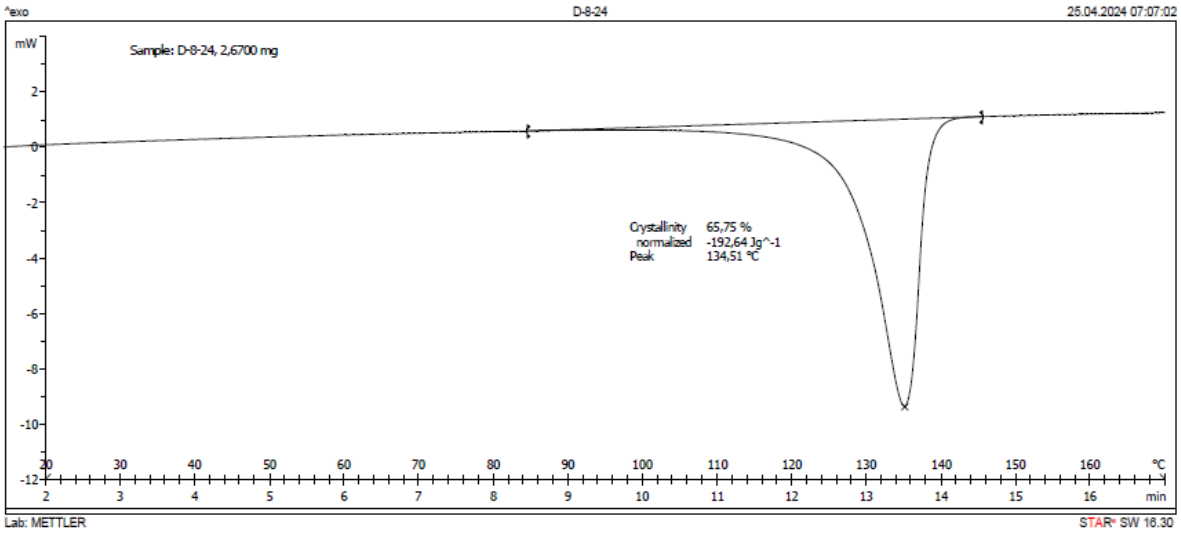

Figure S8. DSC thermogram recorded for polyethylene (entry D-8-24) synthesized with $VO(acac)_2$(4-phenylpiridyne)/Et_2AlCl.

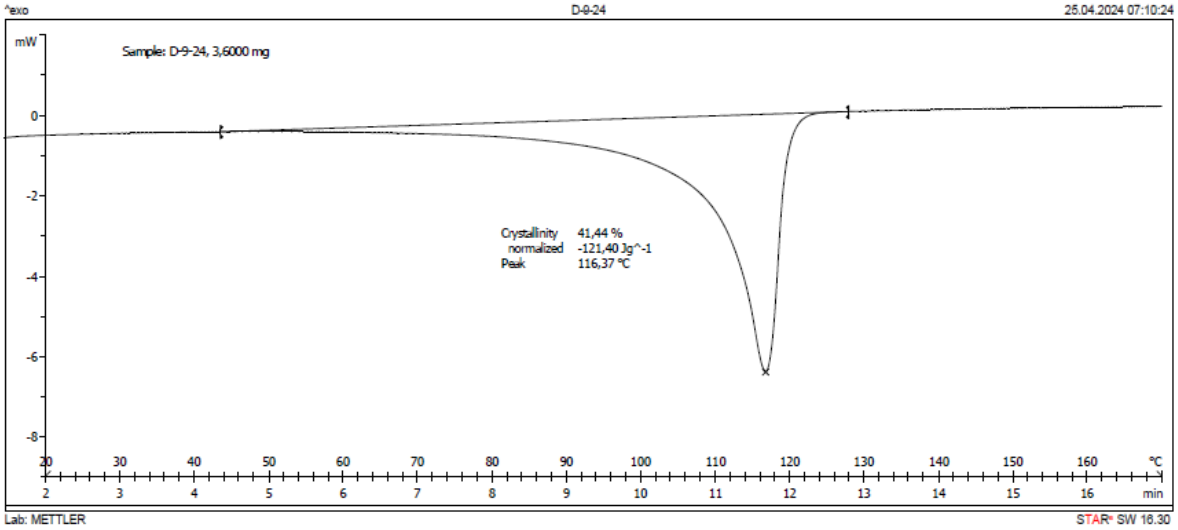

Figure S9. DSC thermogram recorded for ethylene/1-octene copolymer (entry D-9-24) synthesized with $VO(acac)_2$(4-phenylpiridyne)/Et_2AlCl.

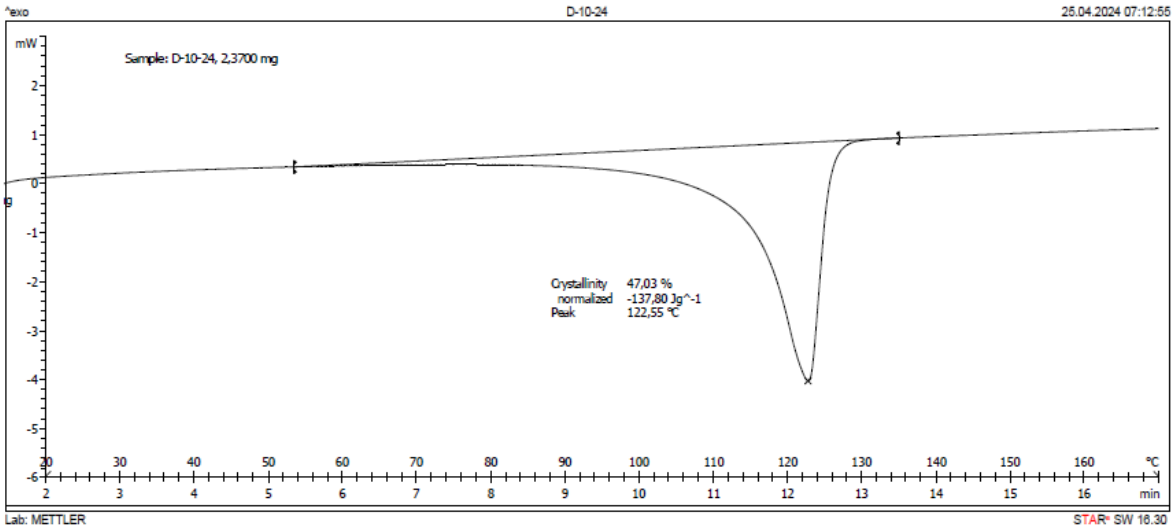

Figure S10. DSC thermogram recorded for ethylene/1-octene copolymer (entry D-10-24) synthesized with $VO(acac)_2$(4-phenylpiridyne)/Et_2AlCl.

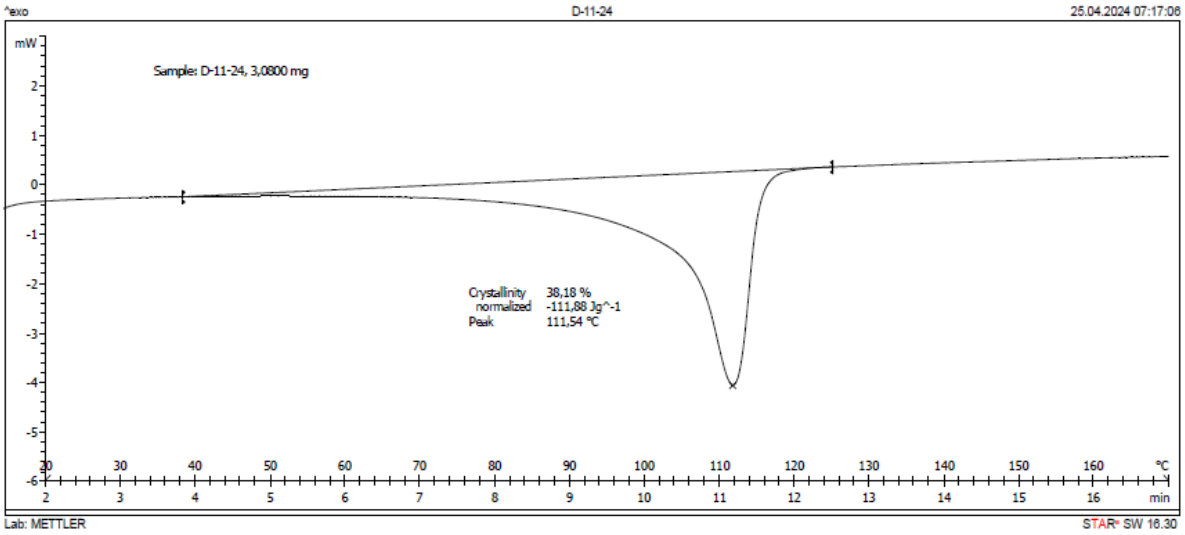

Figure S11. DSC thermogram recorded for ethylene/1-octene copolymer (entry D-11-24) synthesized with $VO(acac)_2$(4-phenylpiridyne)/Et_2AlCl.

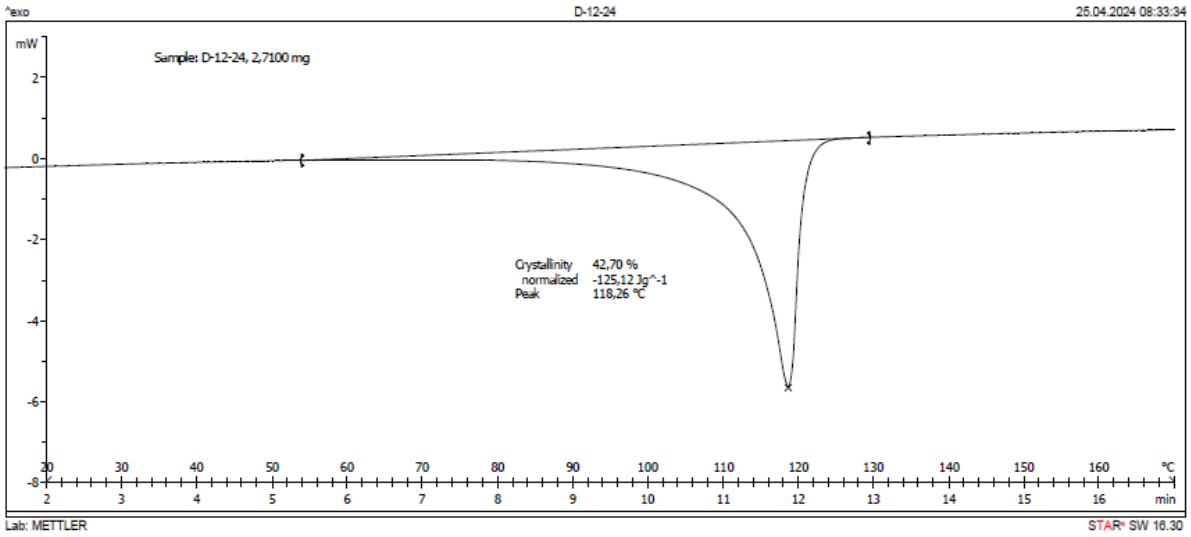

Figure S12. DSC thermogram recorded for ethylene/1-octene copolymer (entry D-12-24) synthesized with $VO(acac)_2$(4-phenylpiridyne)/Et_2AlCl.

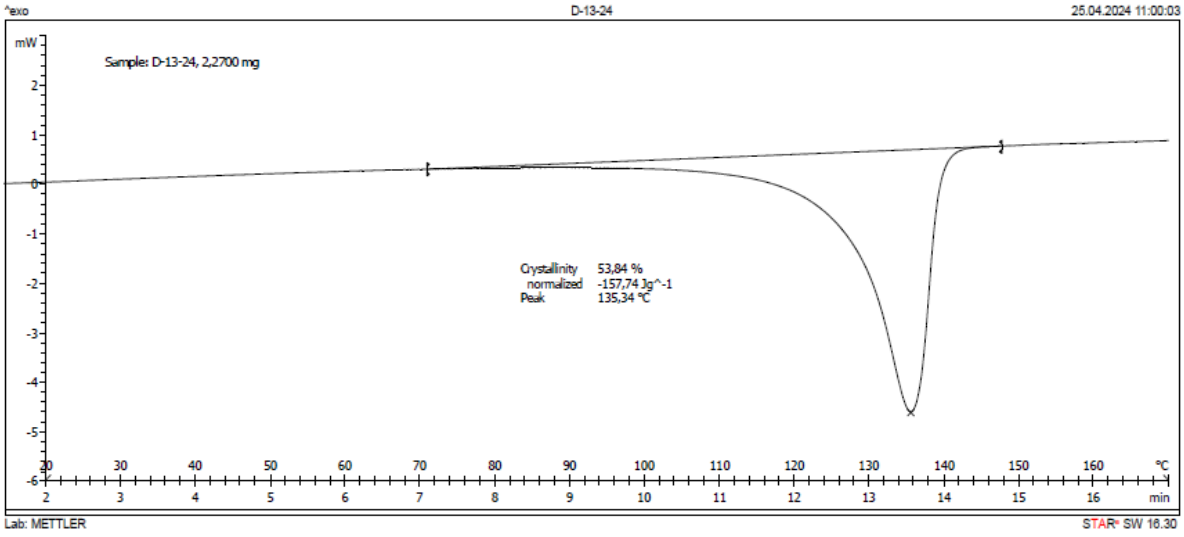

Figure S13. DSC thermogram recorded for polyethylene (entry D-13-24) synthesized with $VO(acac)_2$(4-phenylpiridyne)/$EtAlCl_2$.

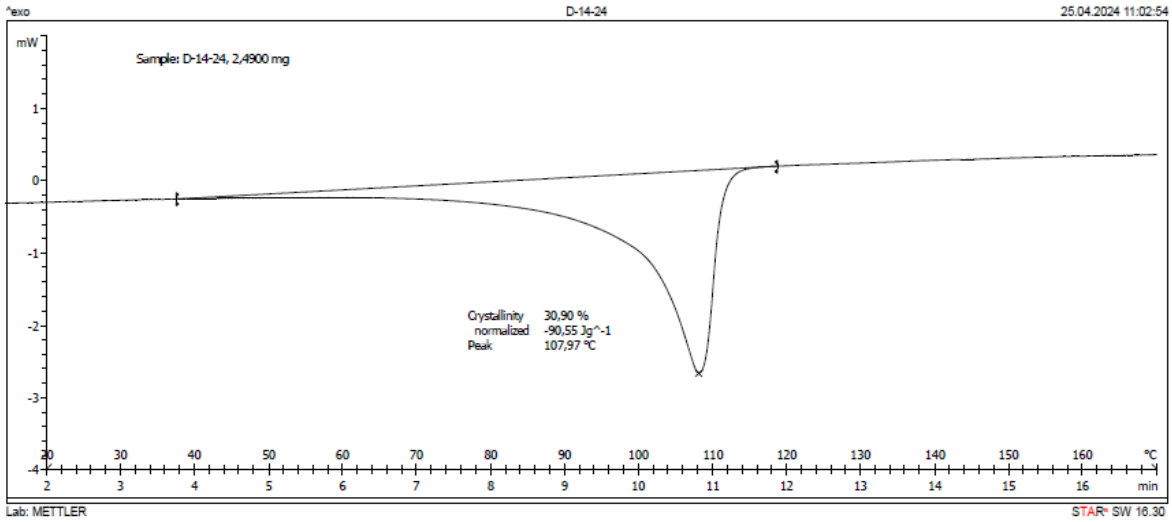

Figure S14. DSC thermogram recorded for ethylene/1-octene copolymer (entry D-14-24) synthesized with $VO(acac)_2$(4-phenylpiridyne)/$EtAlCl_2$.

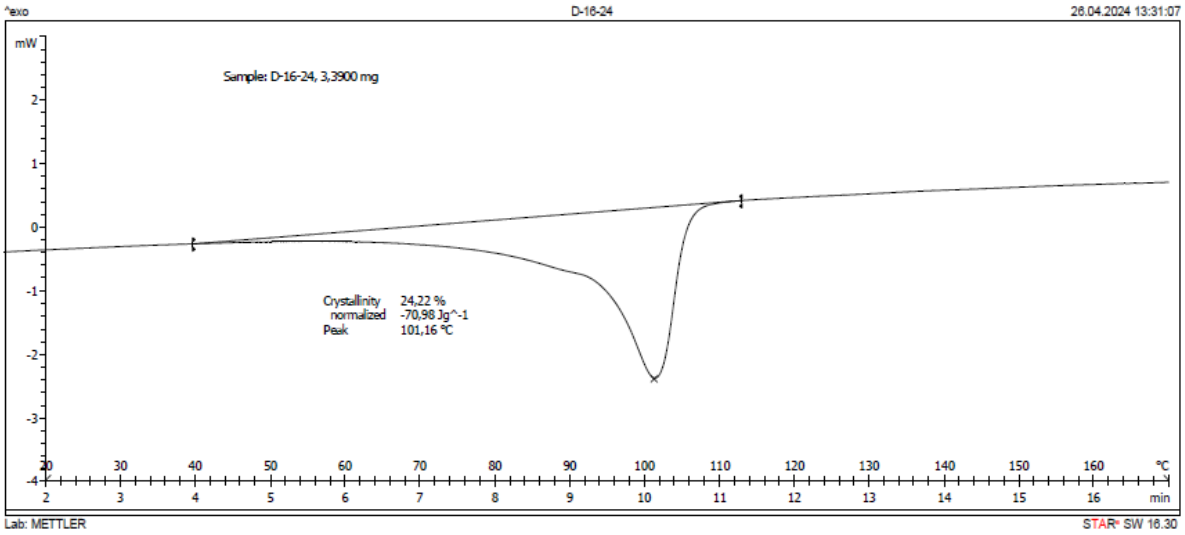

Figure S15. DSC thermogram recorded for ethylene/1-octene copolymer (entry D-16-24) synthesized with $VO(acac)_2$(4-phenylpiridyne)/$EtAlCl_2$.

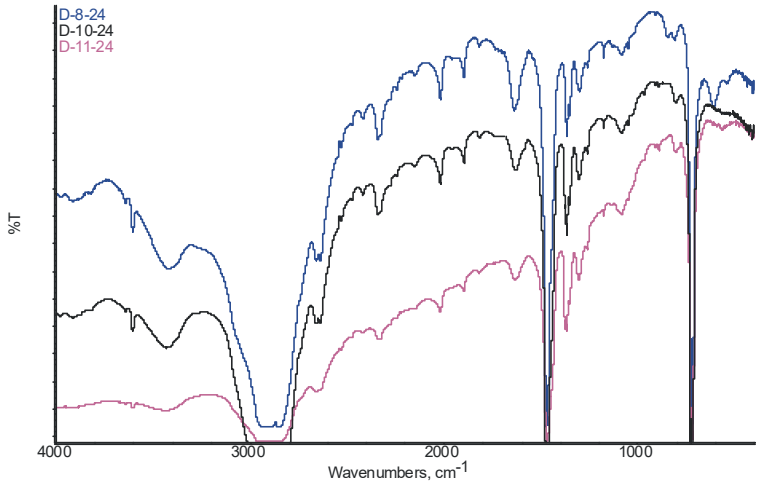

Figure S16. Exemplary full FTIR spectra of PE and ethylene/1-octene copolymers synthesized with $VO(acac)_2$(4-phenylpiridyne)/Et_2AlCl

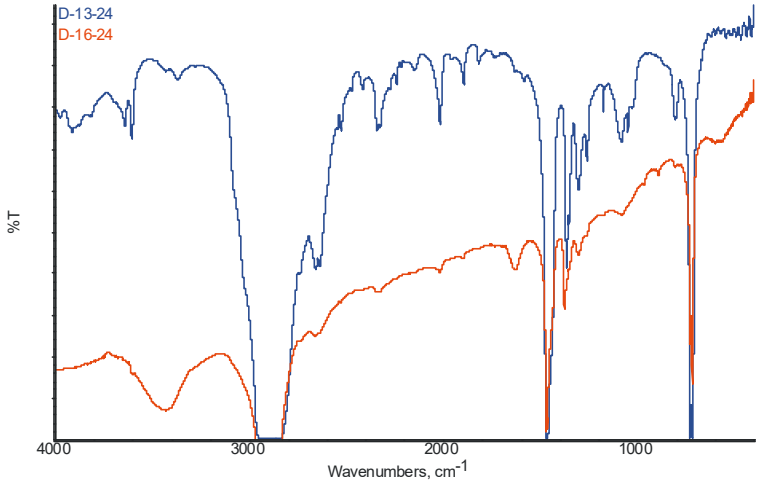

Figure S17. Full FTIR spectra of PE and ethylene/1-octene copolymer synthesized with $VO(acac)_2$(4-phenylpiridyne)/$EtAlCl_2$

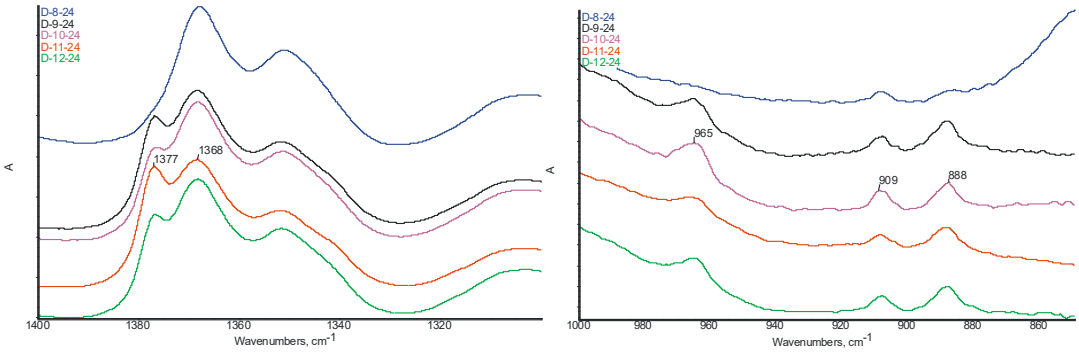

a) b)

Figure S18. FTIR spectra of PE and ethylene/1-octene copolymers synthesized with $VO(acac)_2$(4-phenylpiridyne)/Et_2AlCl: (a) expanded region 1300 cm^{-1} - 1400 cm^{-1} and (b) expanded region 850 cm^{-1}- 1000 cm^{-1}

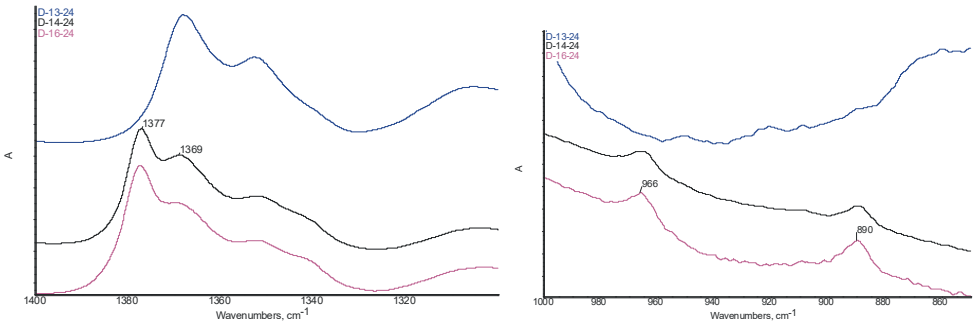

a) b)

Figure S19. Full FTIR spectra of PE and ethylene/1-octene copolymer synthesized with $VO(acac)_2$(4-phenylpiridyne)/$EtAlCl_2$: (a) expanded region 1300 cm^{-1} - 1400 cm^{-1} and (b) expanded region 850 cm^{-1}- 1000 cm^{-1}

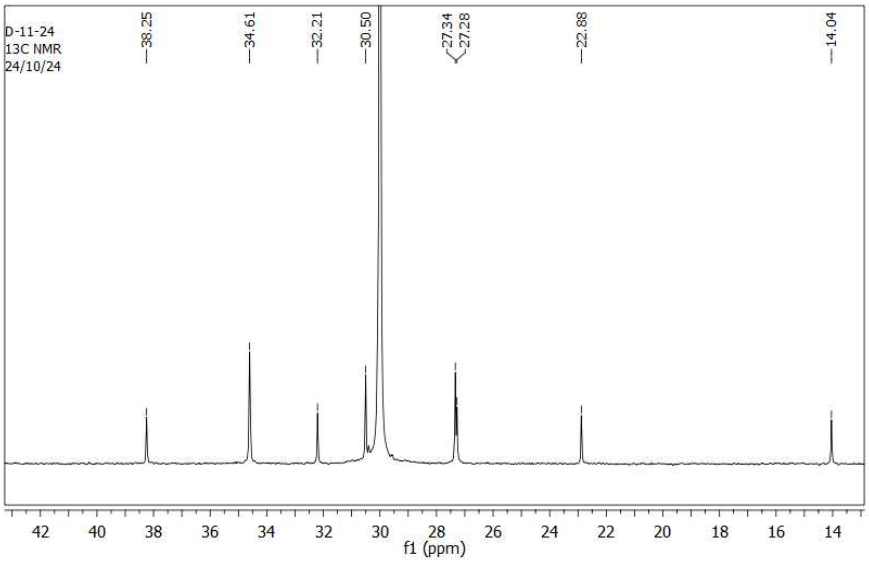

Figure S20. $^{13}C\{^1H\}$ NMR spectrum of the copolymer produced by $VO(acac)_2$(4-phenylpiridyne)/$EtAlCl_2$ (D-11-24).

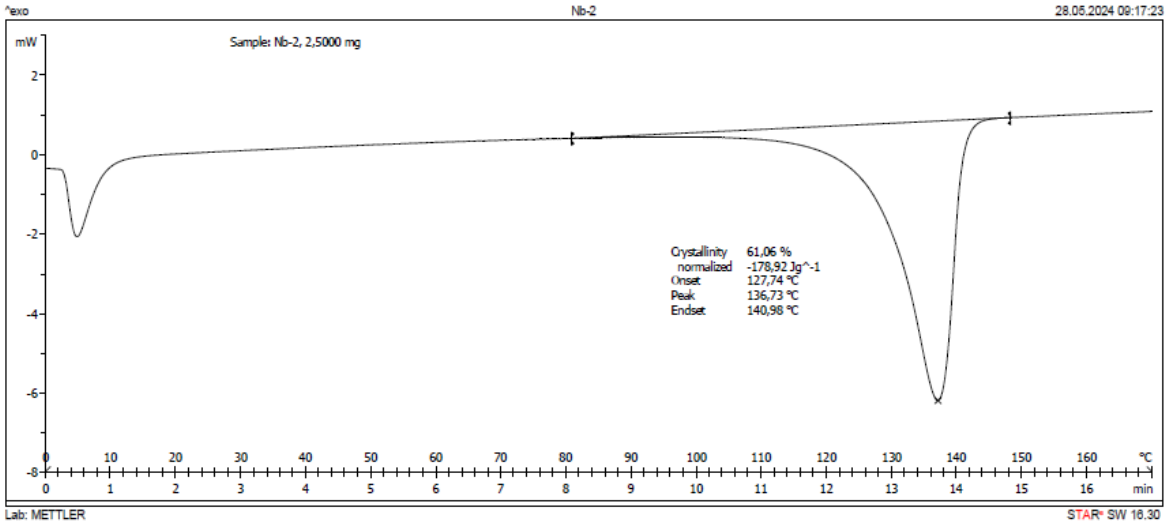

Figure S21. DSC thermogram recorded for polyethylene (entry Nb-2) synthesized with niobium compound/Et_2AlCl.

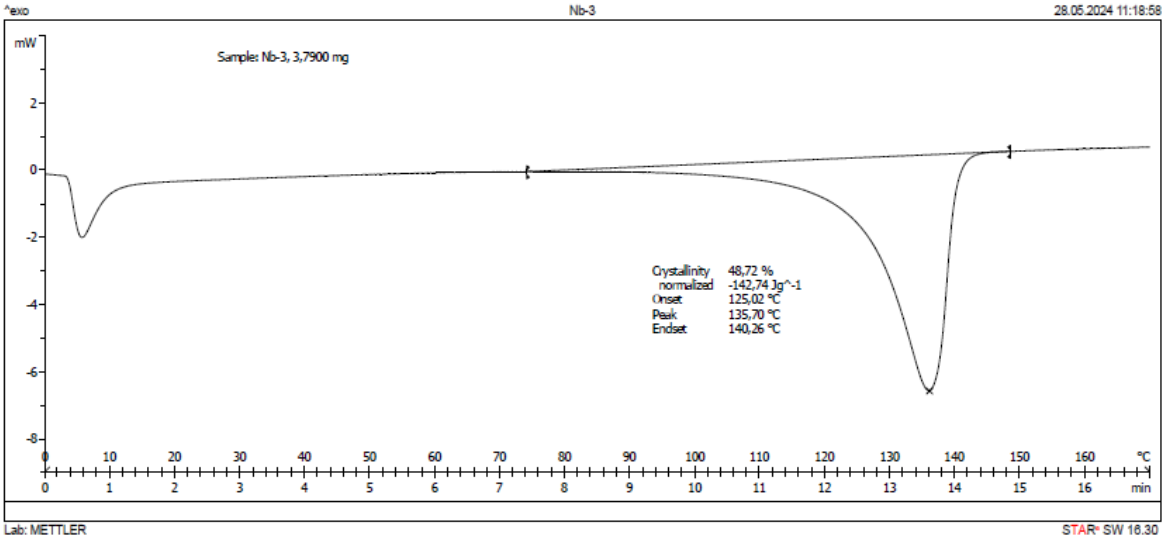

Figure S22. DSC thermogram recorded for polyethylene (entry Nb-3) synthesized with niobium compound/$EtAlCl_2$.

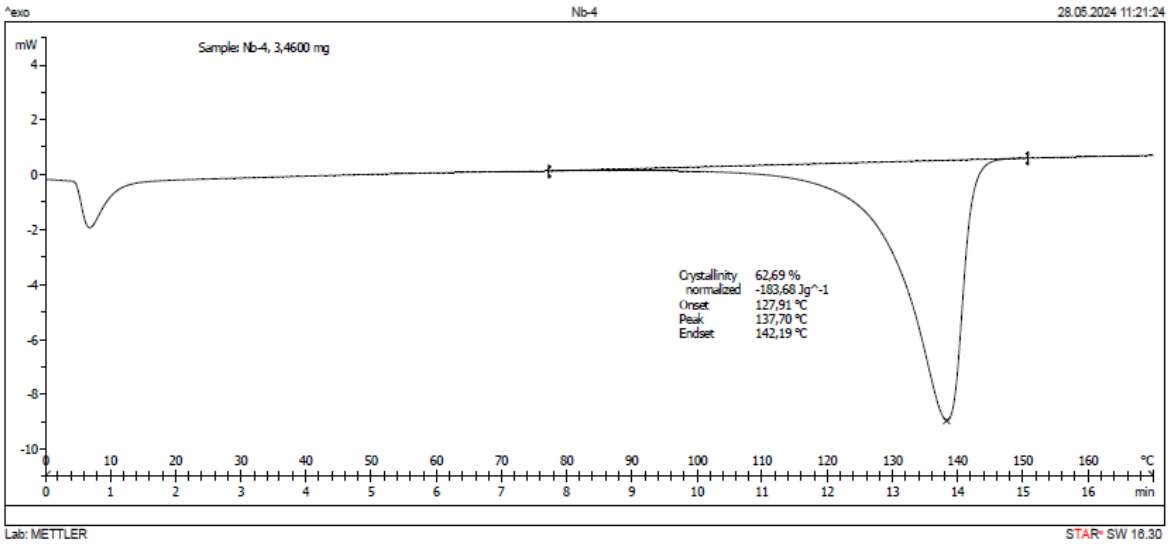

Figure S23. DSC thermogram recorded for polyethylene (entry Nb-4) synthesized with niobium compound/Et_2AlCl.

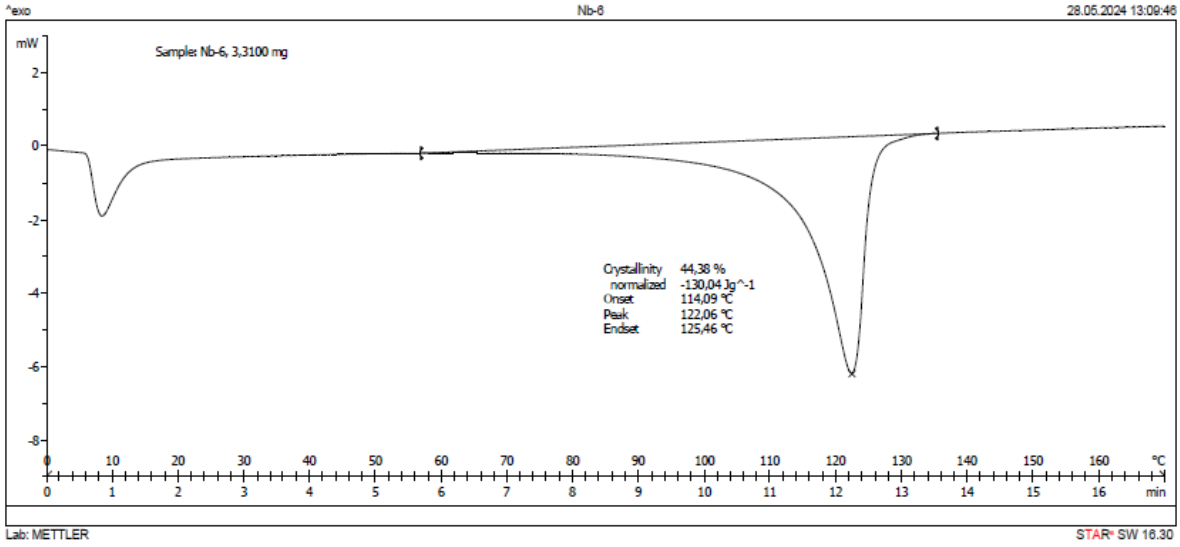

Figure S24. DSC thermogram recorded for ethylene/1-octene copolymer (entry Nb-6) synthesized with niobium compound/Et_2AlCl.

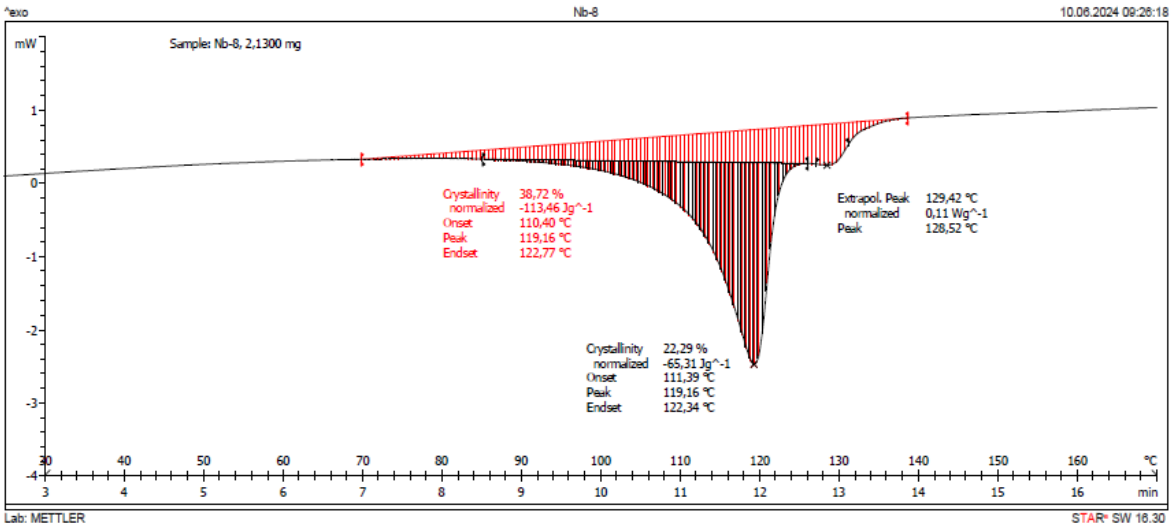

Figure S25. DSC thermogram recorded for ethylene/1-octene copolymer (entry Nb-8) synthesized with niobium compound/Et_2AlCl.

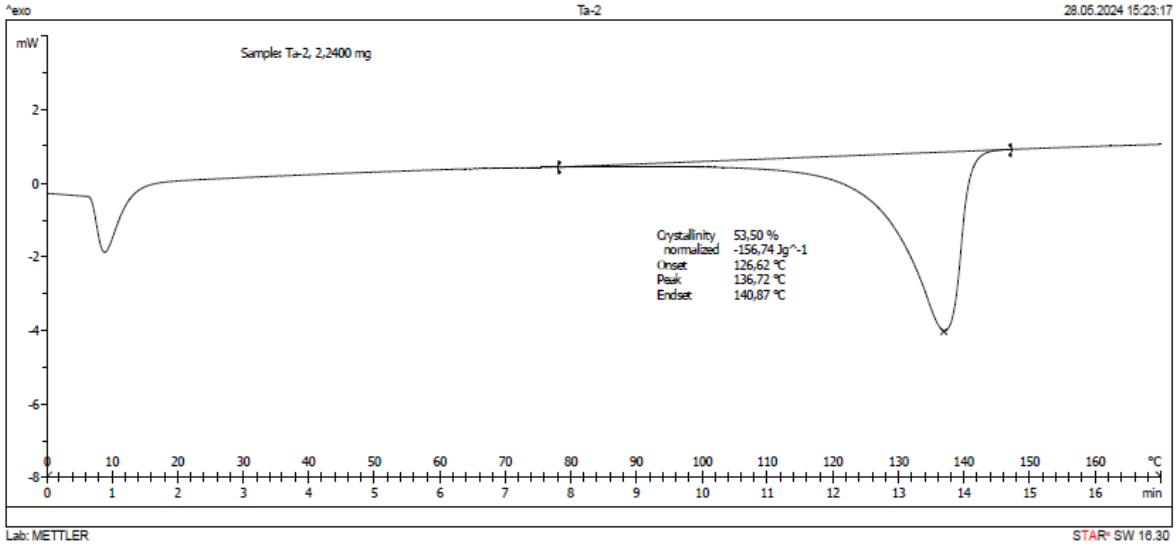

Figure S26. DSC thermogram recorded for polyethylene (entry Ta-2) synthesized with tantalum compound/$EtAlCl_2$.

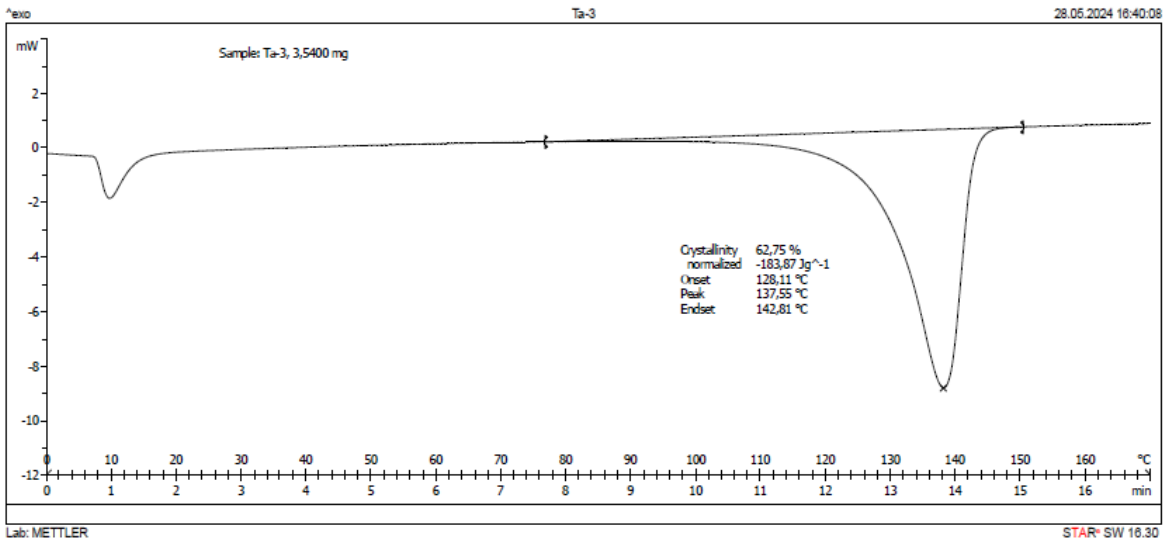

Figure S27. DSC thermogram recorded for polyethylene (entry Ta-3) synthesized with tantalum compound/Et_2AlCl.

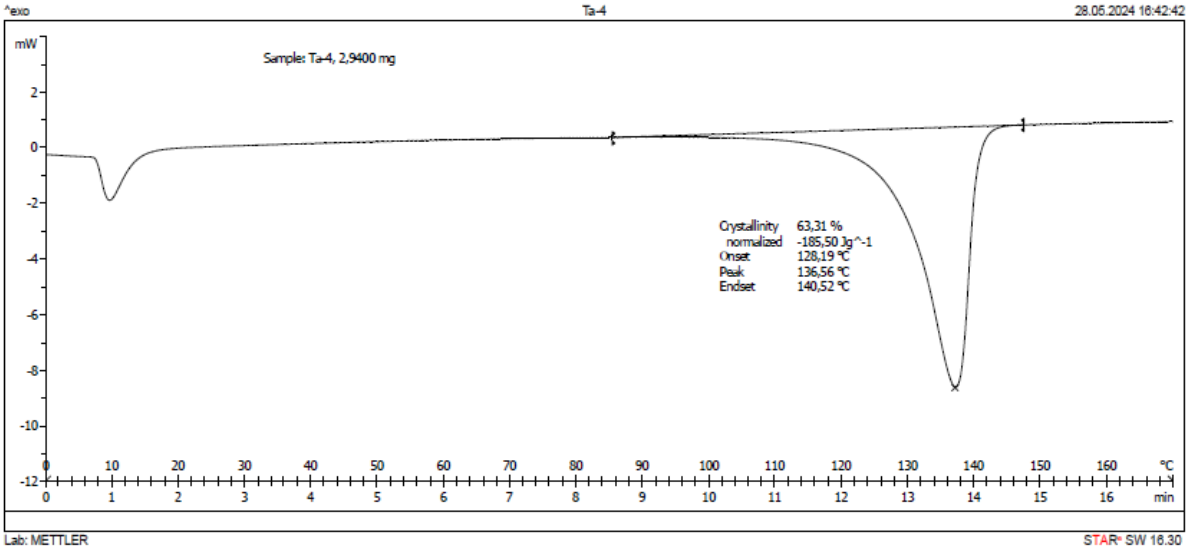

Figure S28. DSC thermogram recorded for polyethylene (entry Ta-4) synthesized with tantalum compound/Et_2AlCl.

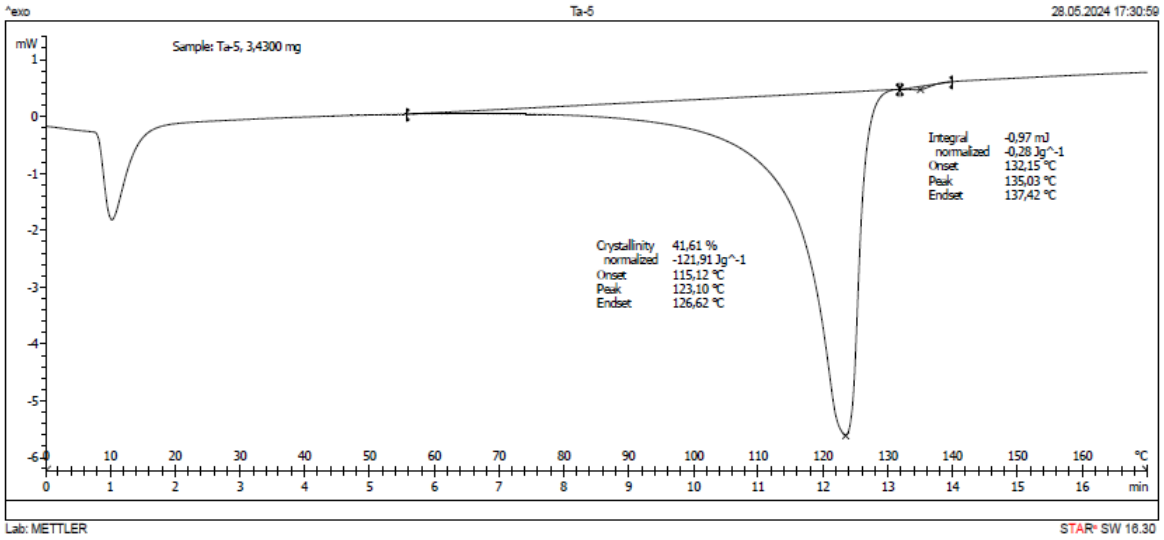

Figure S29. DSC thermogram recorded for ethylene/1-octene copolymer (entry Ta-5) synthesized with tantalum compound/Et_2AlCl.

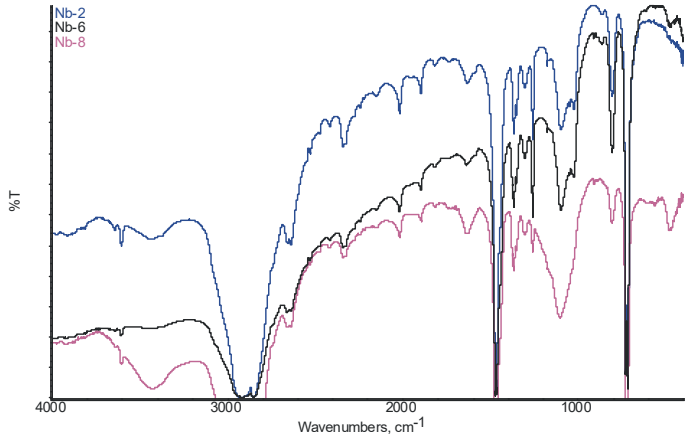

Figure S30. Exemplary full FTIR spectra of PE and ethylene/1-octene copolymers synthesized with niobium catalyst.

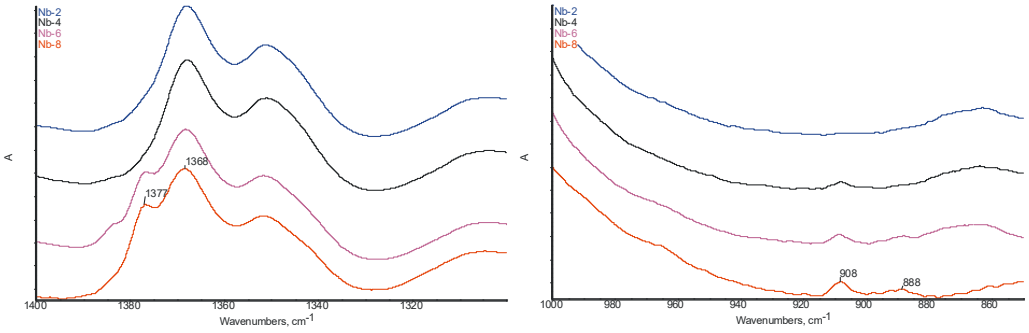

a) b)

Figure S31. FTIR spectra of PE and ethylene/1-octene copolymers synthesized with niobium catalyst: (a) expanded region 1300 cm^{-1} - 1400 cm^{-1} and (b) expanded region 850 cm^{-1}- 1000 cm^{-1}

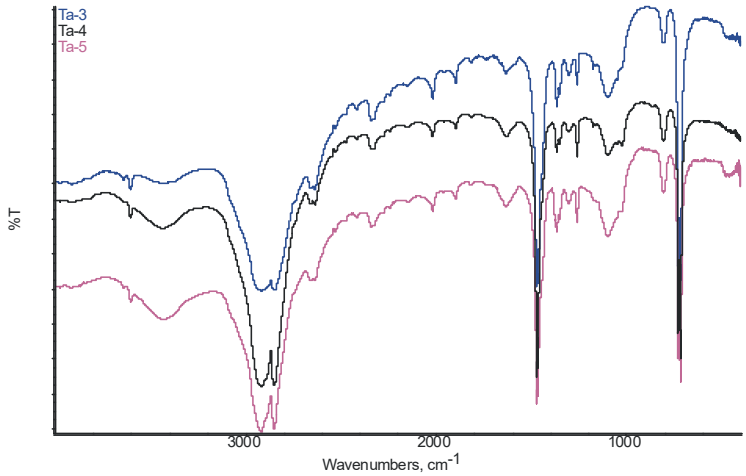

Figure S32. Exemplary full FTIR spectra of PE and ethylene/1-octene copolymers synthesized with tantalum catalysts.

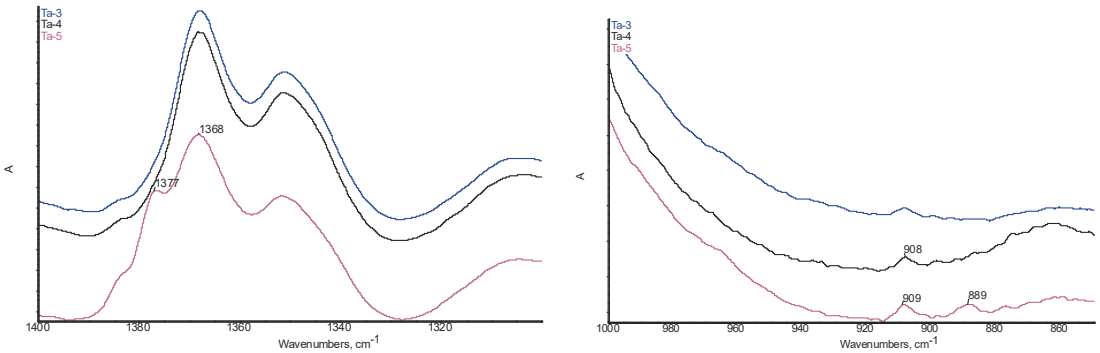

a) b)

Figure S33. FTIR spectra of PE and ethylene/1-octene copolymers synthesized with tantalum catalyst: (a) expanded region 1300 - 1400 cm^{-1} and (b) expanded region 850 - 1000 cm^{-1}

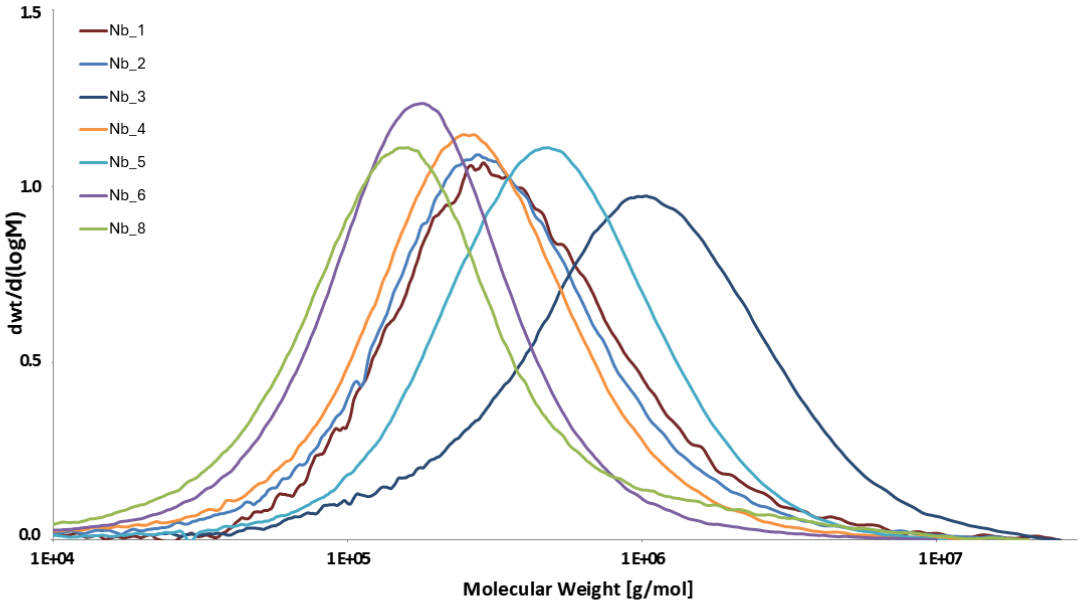

Figure S34. Molecular weight distribution of polyethylenes and ethylene/1-octene copolymers synthesized with niobium catalysts

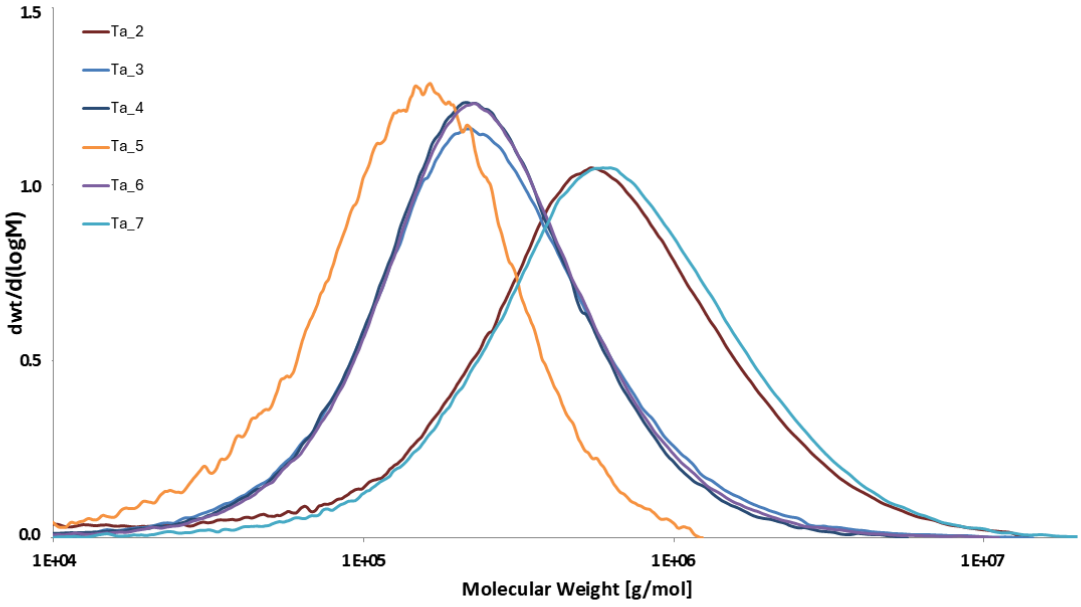

Figure S35. Molecular weight distribution of polyethylenes and ethylene/1-octene copolymer synthesized with tantalum catalysts

Table S5. Results of preparation of self-healing materials based on methyl methacrylate catalyzed by V(IV), Nb(V) or Ta(V) complex compound *via* Et_2AlCl as activator

Entry	Al/V(Nb,Ta) molar ratio	Amount of MMA used for the process (% of the total volume of the starting reaction mixture)	A [a)]	Tg (°C)[b)]	M_w/M_n [c)]
V-PE-20MMA	1:1500	20%	38192	36	1.26
V-PE-30MMA	1:1500	30%	48572	30	1.14
V-PE-50MMA	1:1500	50%	92137	33	1.39
Nb-PE-20MMA	1:1500	20%	63289	60	1.03
Nb-PE-30MMA	1:1500	30%	81724	31	1.15
Nb-PE-50MMA	1:1500	50%	29481	27	1.01
Ta-PE-20MMA	1:1500	20%	52943	60	1.04
Ta-PE-30MMA	1:1500	30%	47813	51	1.02
Ta-PE-50MMA	1:1500	50%	83976	12	1.09

Polymerization conditions: DMSO/toluene, time 15 min, ethylene 1 bar; a) Polymerization activity, $kg \cdot mol^{-1} \cdot h^{-1}$ b) Determined by DSC c) Determined by MALDI-TOF-MS (e.g. Fig. S41-S45)

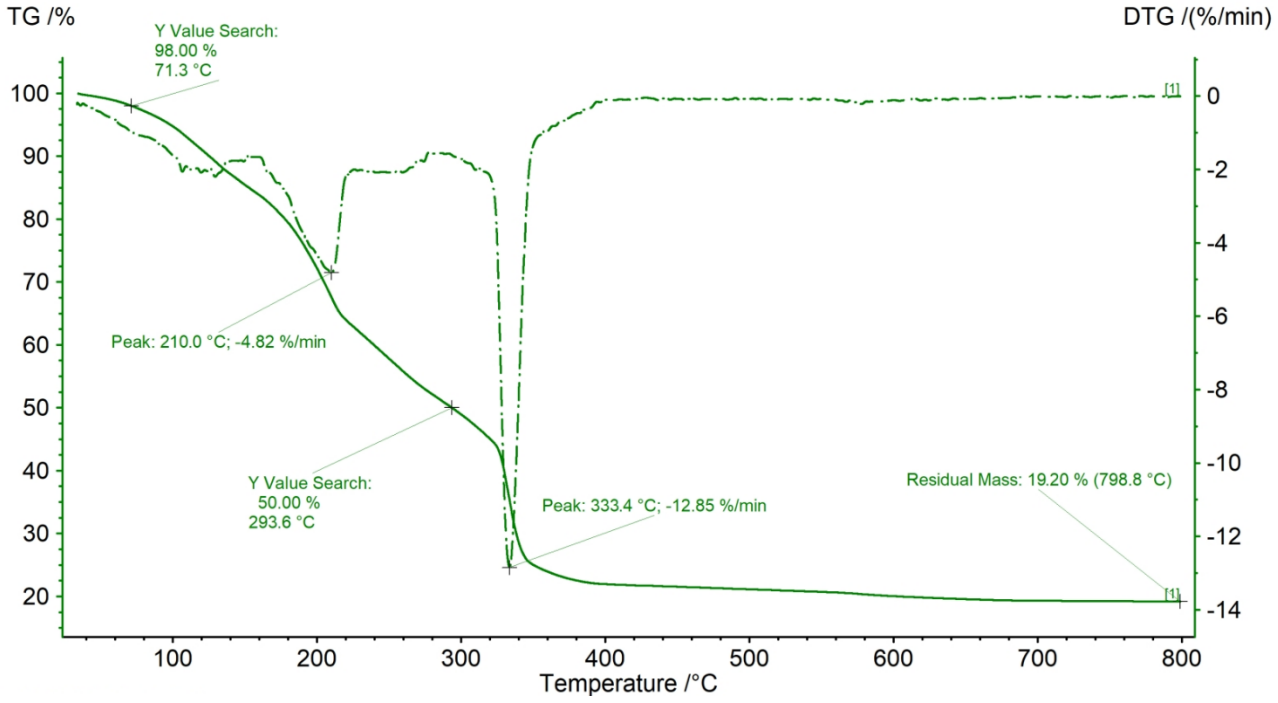

Figure S36. TG/TGA curves for Nb-PE-20MMA

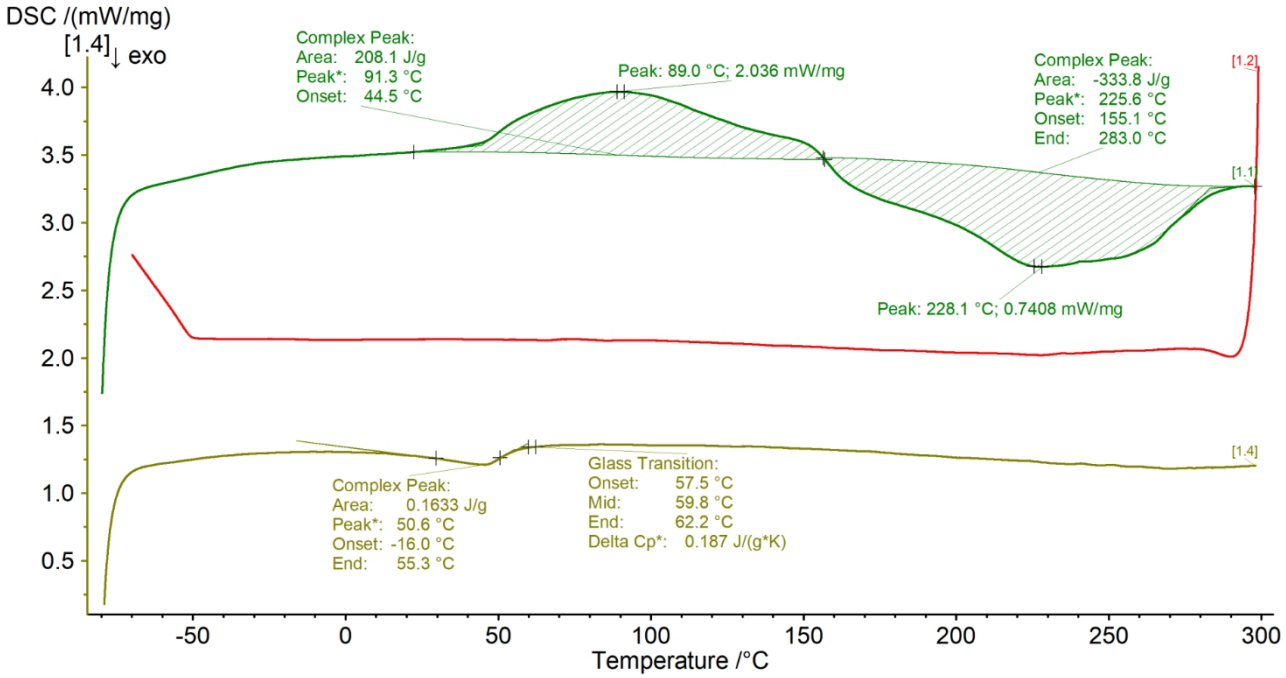

Figure S37. DSC curves for Nb-PE-30MMA

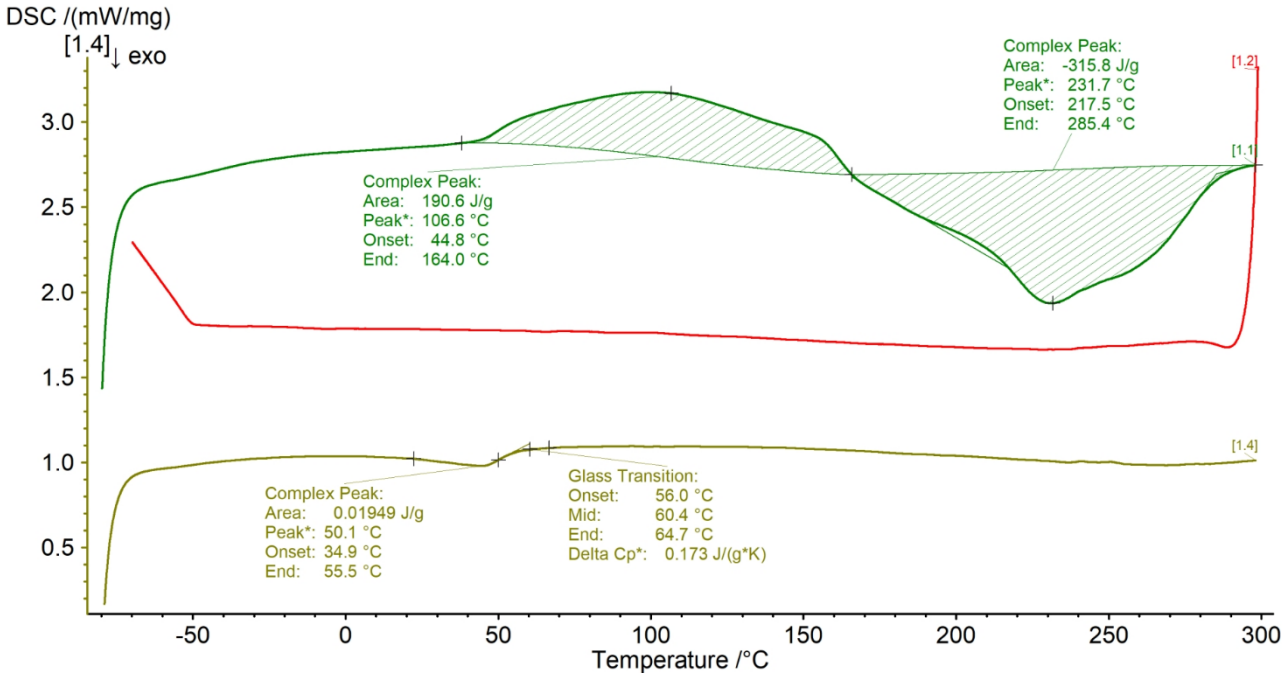

Figure S38. DSC curves for Ta-PE-20MMA

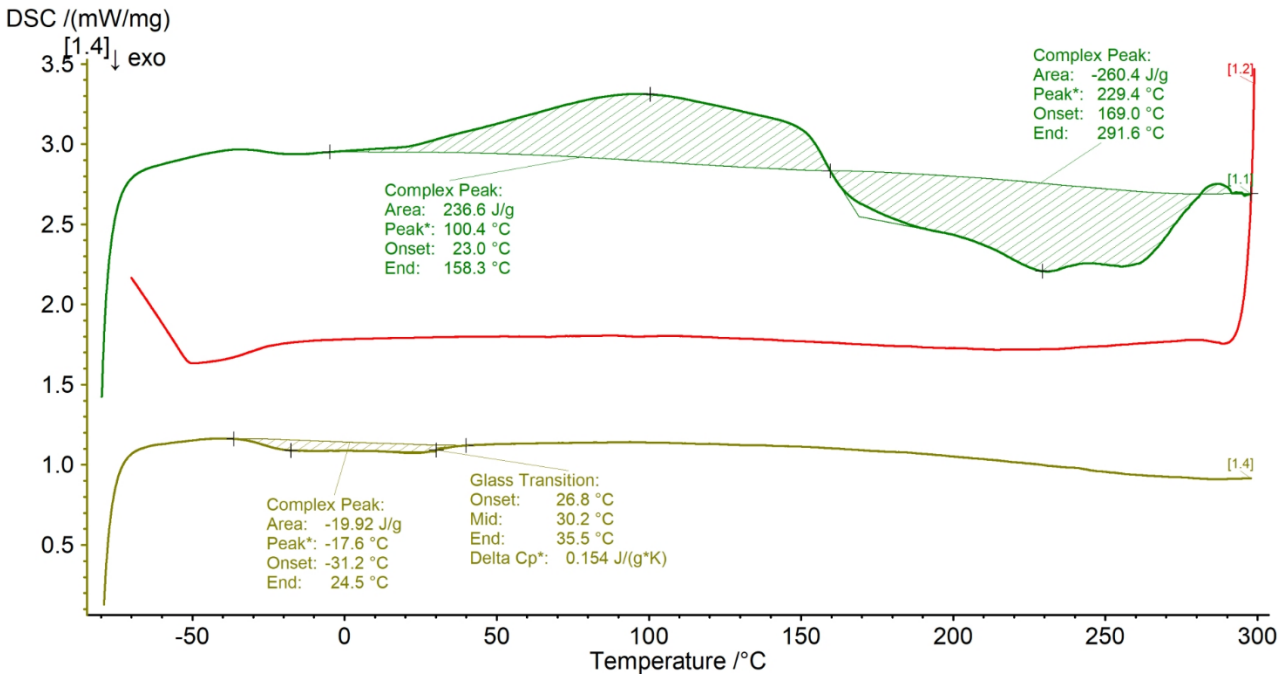

Figure S39. DSC curves for V-PE-30MMA

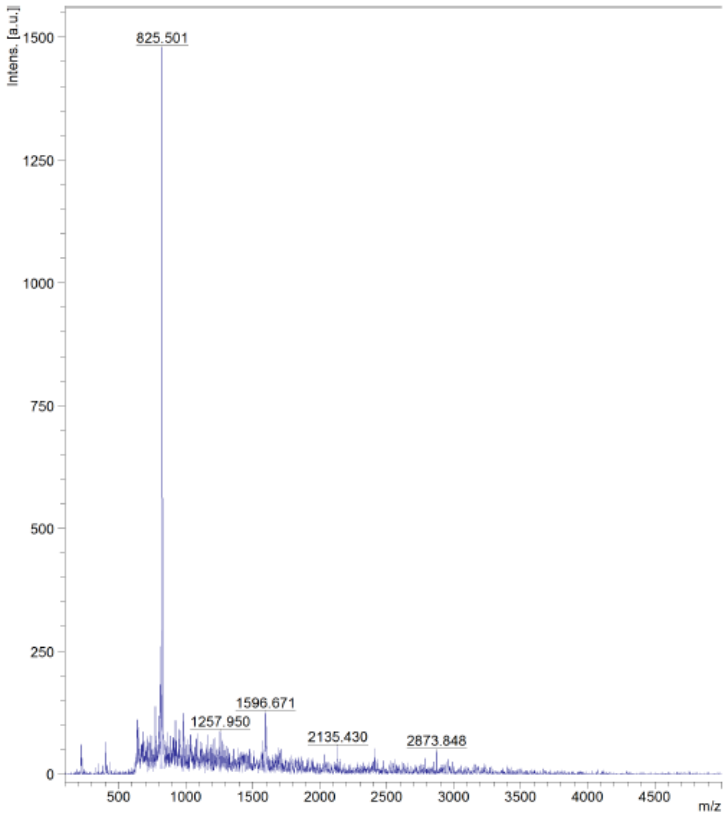

Figure S40. Exemplary MALDI-TOF-MS spectrum for V-PE-20MMA

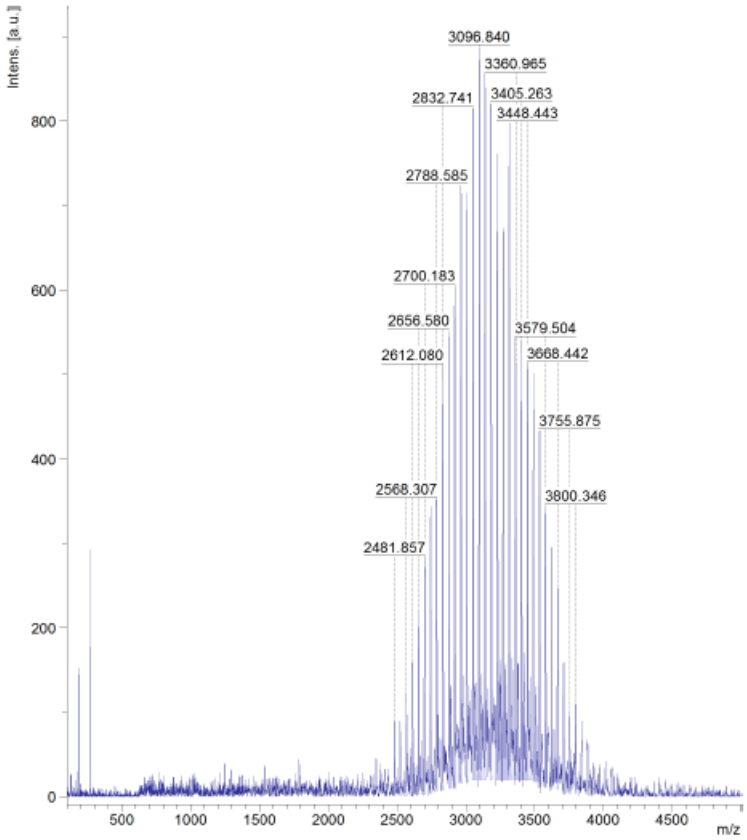

Figure S41. Exemplary MALDI-TOF-MS spectrum for Nb-PE-50MMA

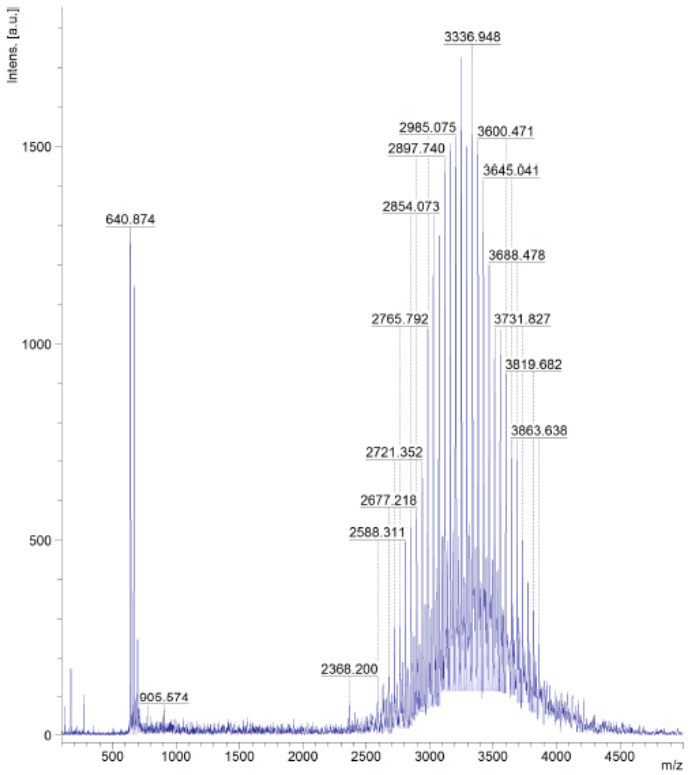

Figure S42. Exemplary MALDI-TOF-MS spectrum for Ta-PE-20MMA

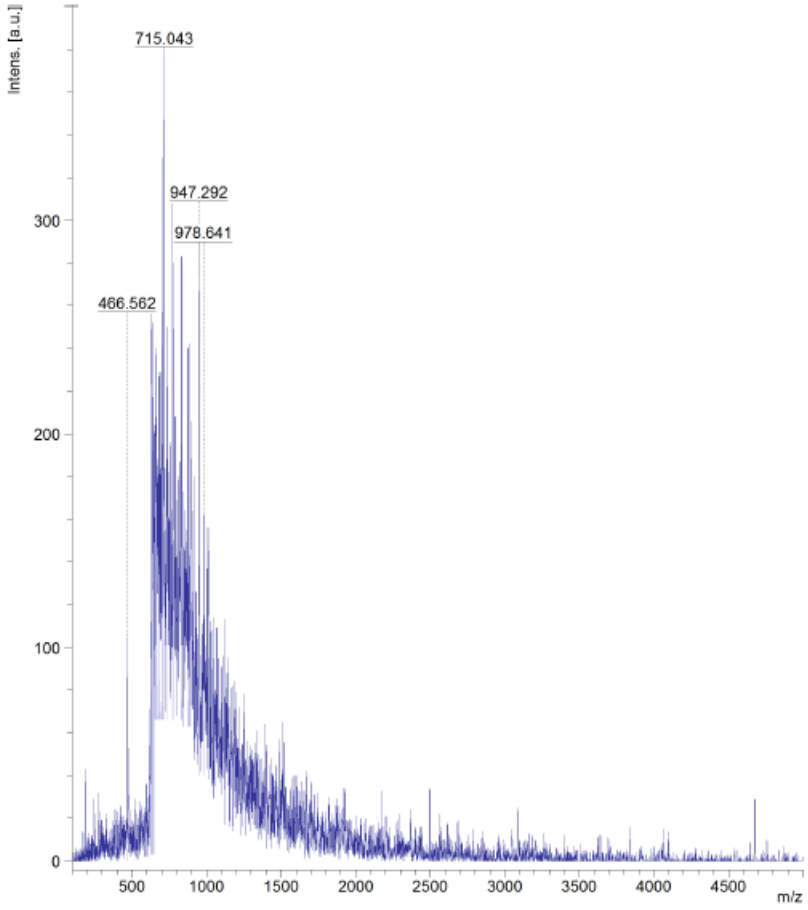

Figure S43. Exemplary MALDI-TOF-MS spectrum for Ta-PE-30MMA

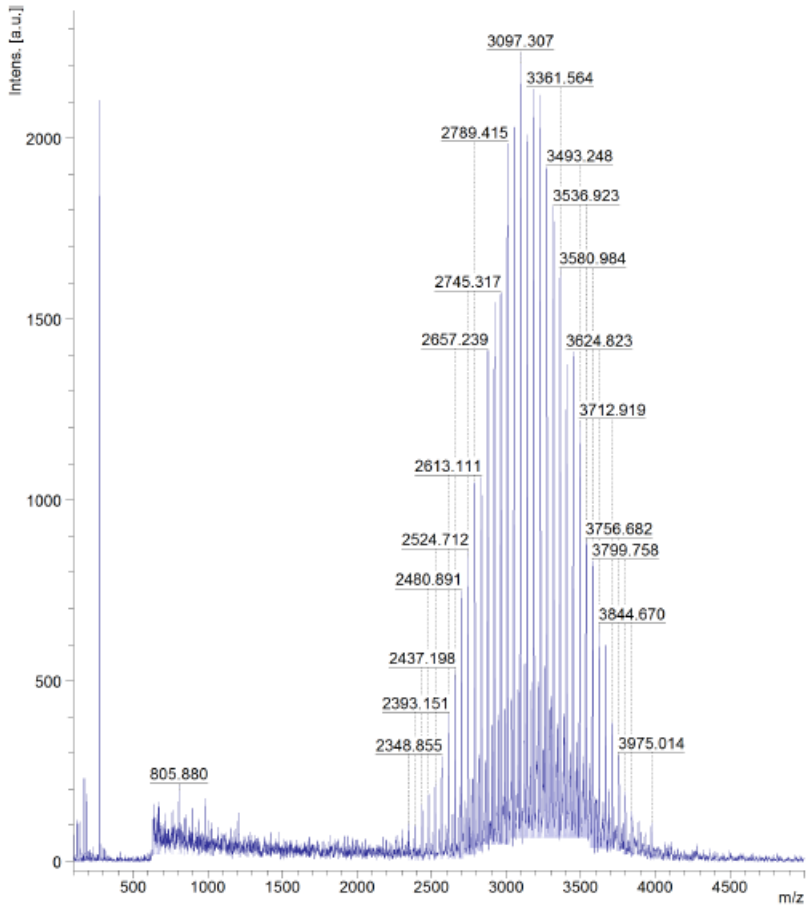

Figure S44. MALDI-TOF-MS spectrum for sample Nb-PE-20MMA.

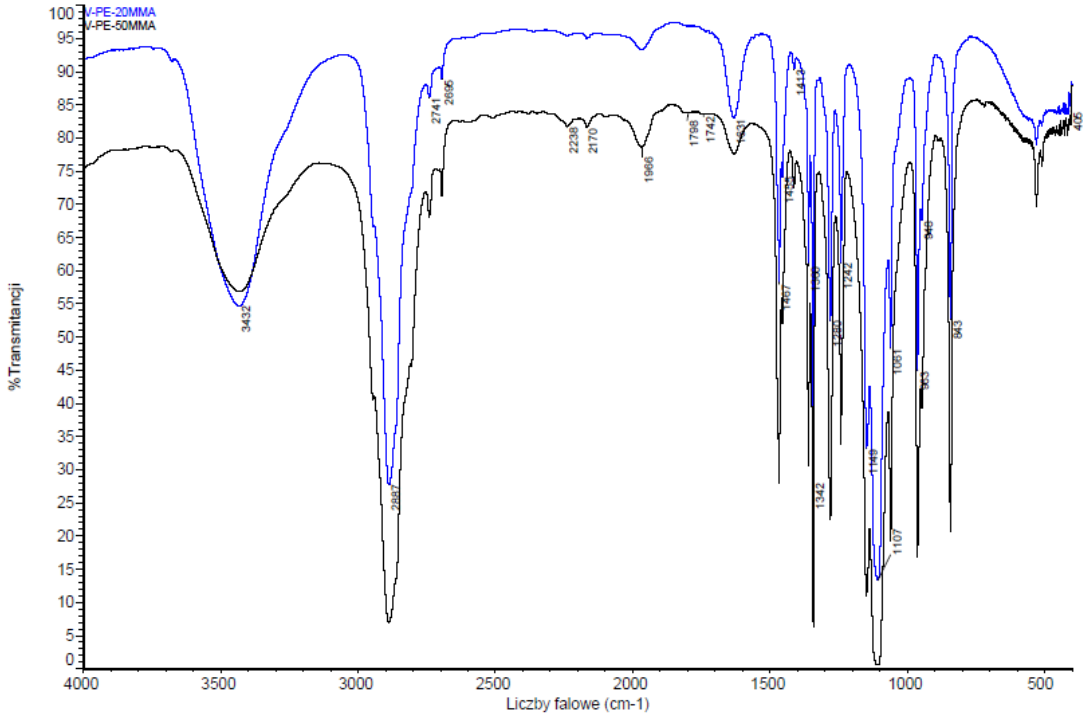

Figure S45. FTIR spectra of samples of self-healing materials obtained using a vanadium-based catalyst.

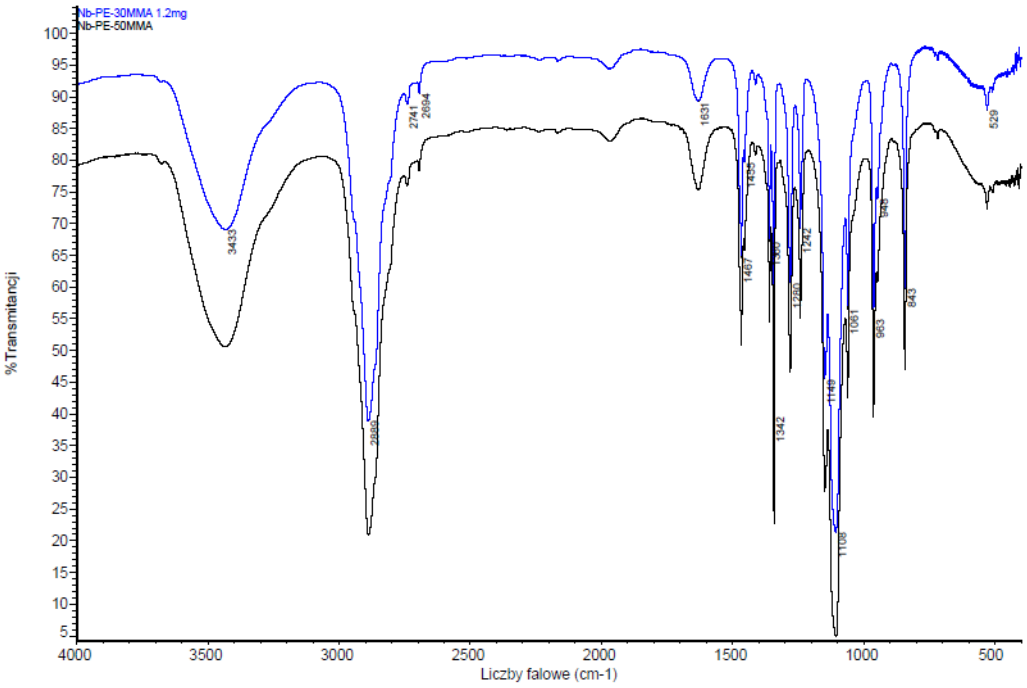

Figure S46. FTIR spectra of samples of self-healing materials obtained using a niobium-based catalyst.

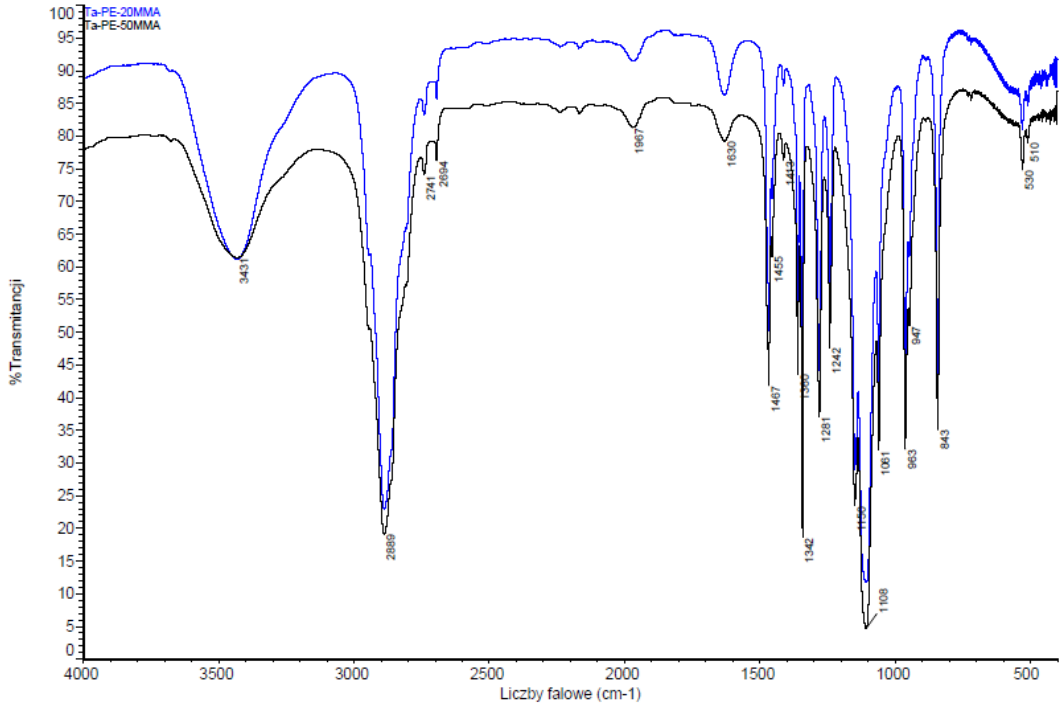

Figure S47. FTIR spectra of samples of self-healing materials obtained using a tantalum-based catalyst.

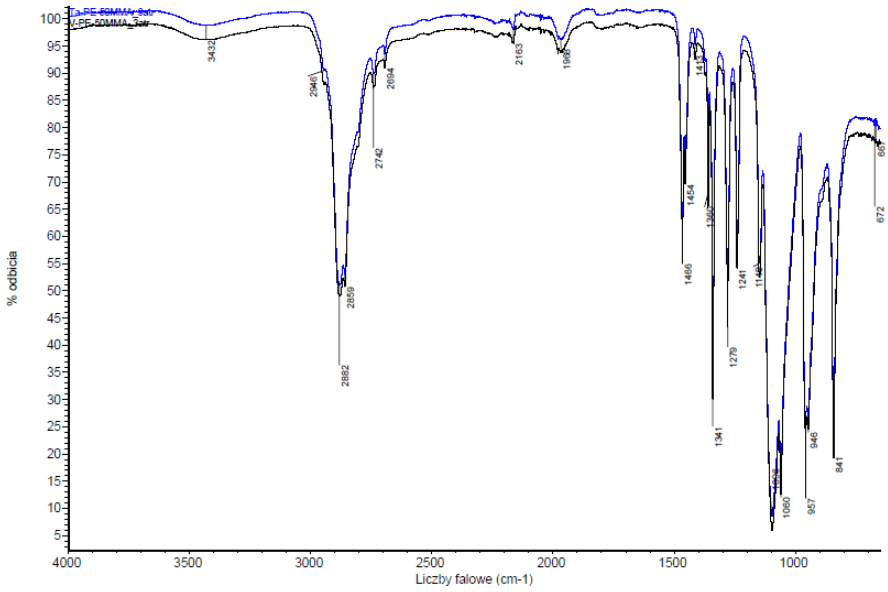

Figure S48. FTIR spectra of samples obtained using vanadium (V-PE-50MMA) and tantalum-based (Ta-PE-50MMA) catalysts (ATR method).

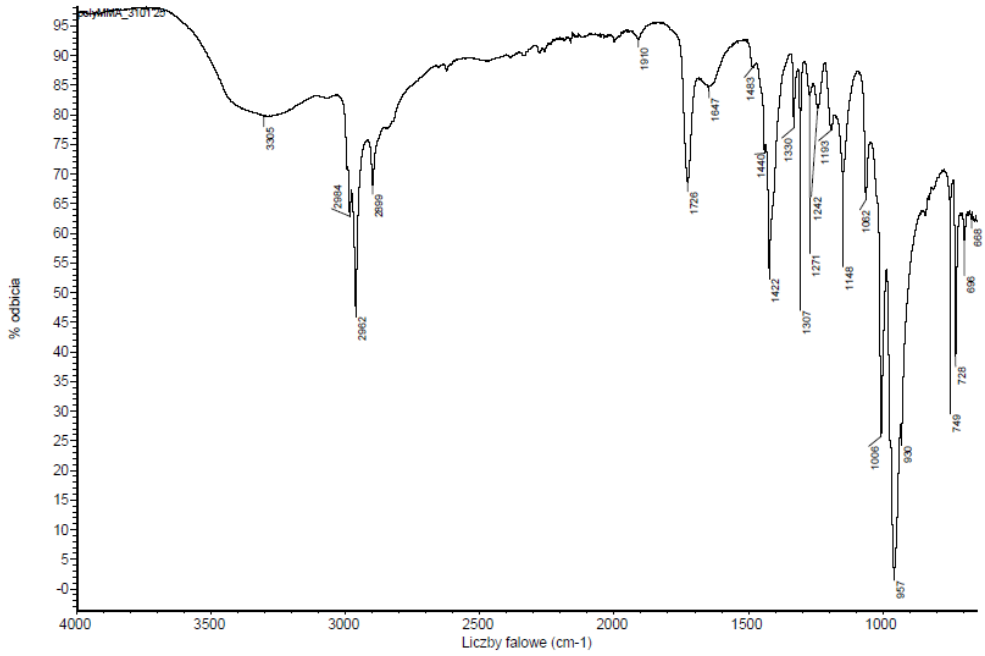

Figure S49. FTIR spectrum of polyMMA sample obtained using a Nb(V)-based catalyst (ATR method).

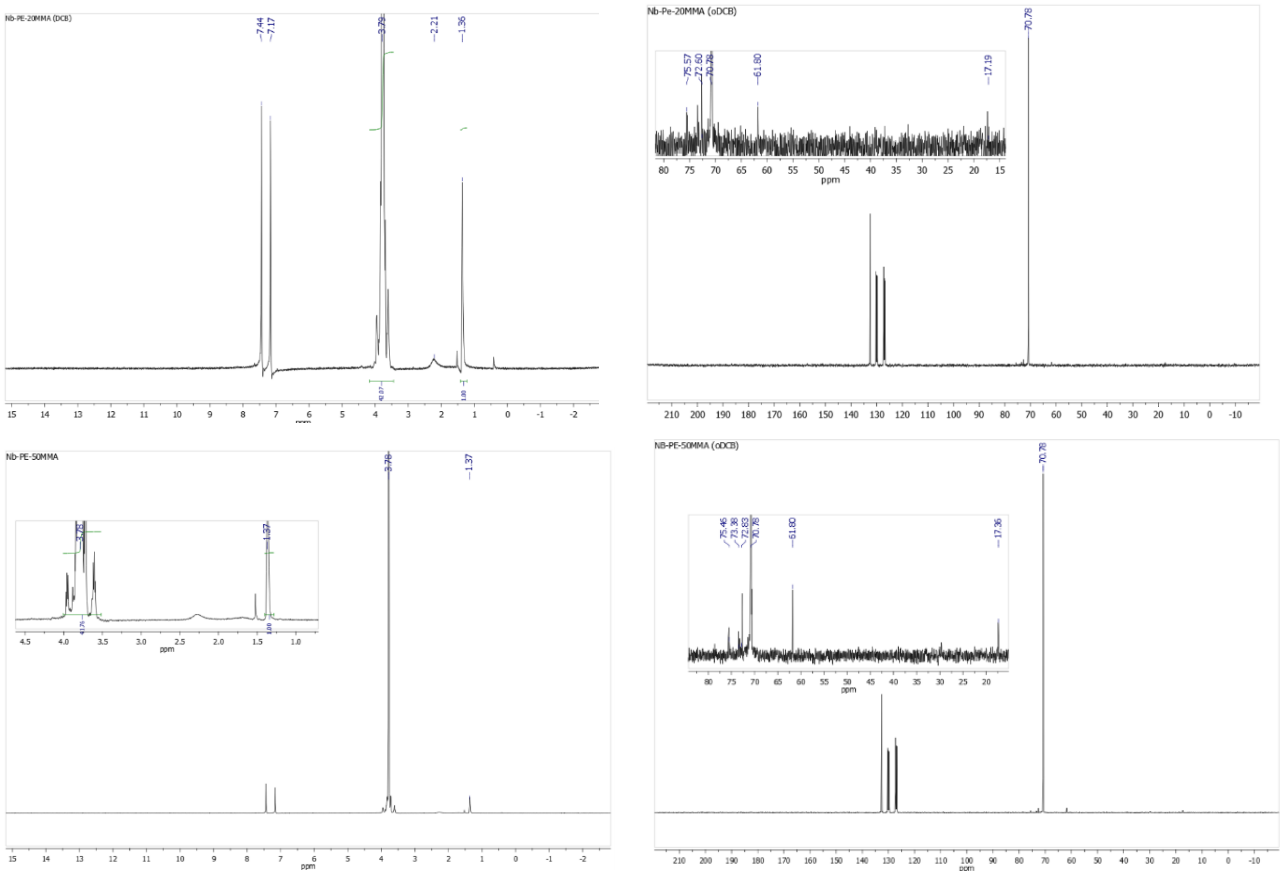

Figure S50. [1]H and [13] C NMR spectra of samples obtained using a niobium-based catalyst (Nb-PE-20MMA and Nb-PE-50MMA, o-dichlorobenzene-d4 as a solvent).

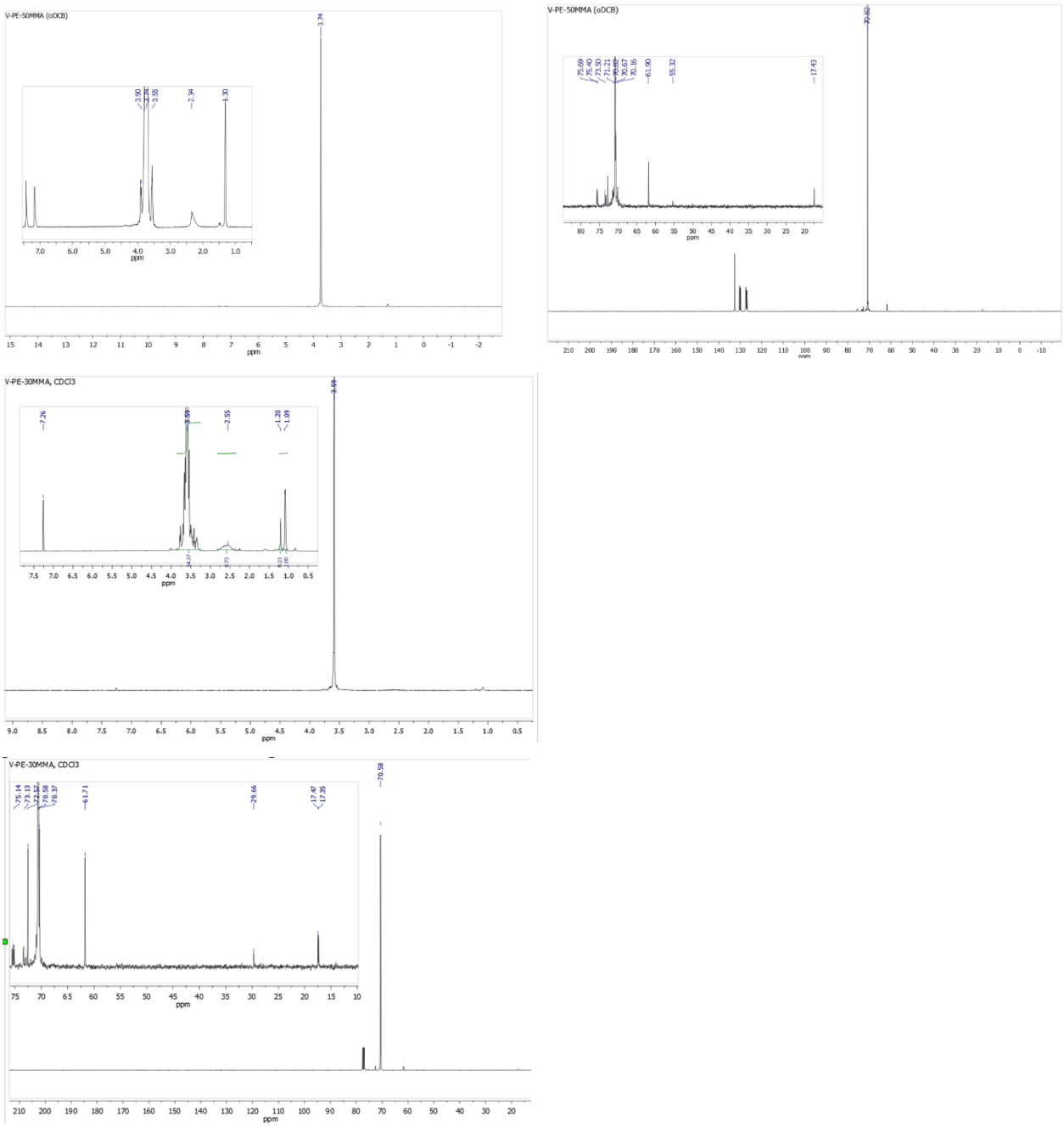

Figure S51. ^{1}H and ^{13} C NMR spectra of samples obtained using a vanadium-based catalyst (V-PE-50MMA, o-dichlorobenzene-d4 as a solvent and V-PE-30MMA, $CDCl_3$ as a solvent).

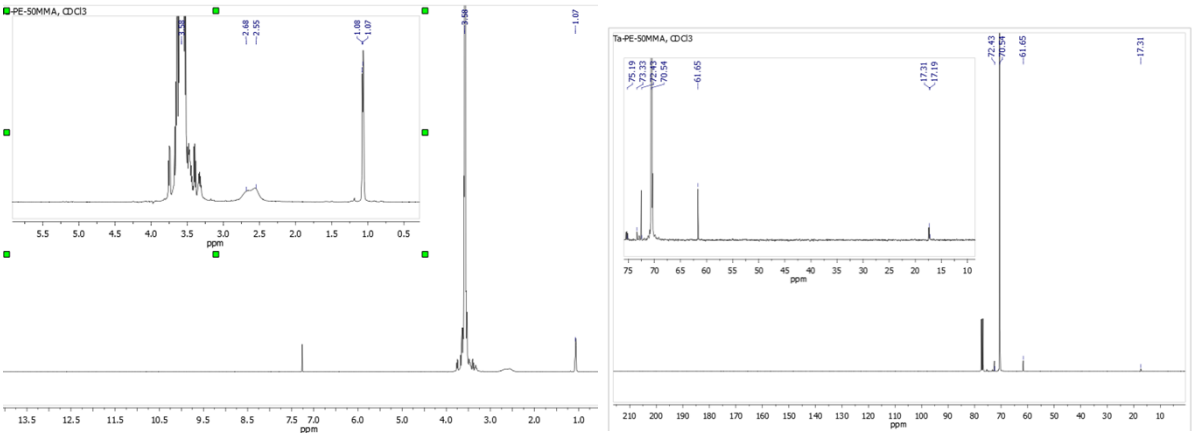

Figure S52. ^{1}H and ^{13}C NMR spectra of samples obtained using a tantalum-based catalyst (Ta-PE-50MMA).

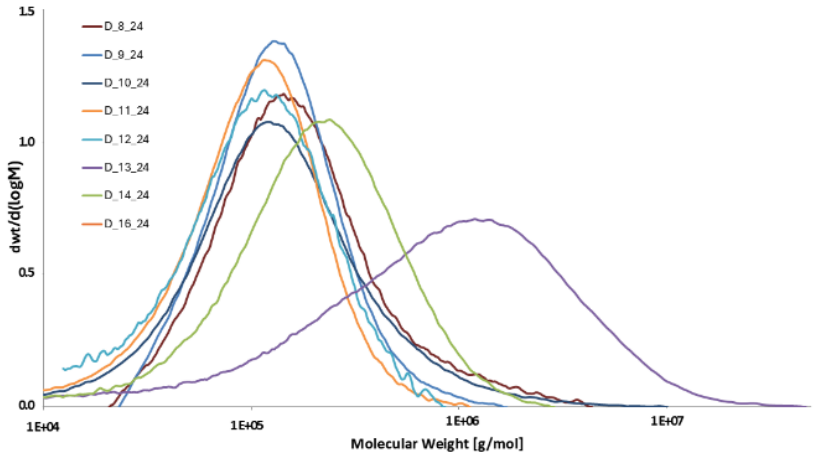

Figure S53. Molecular weight distribution of polyethylenes and ethylene/1-octene copolymers synthesized with $VO(acac)_2$(4-phenylpiridyne).

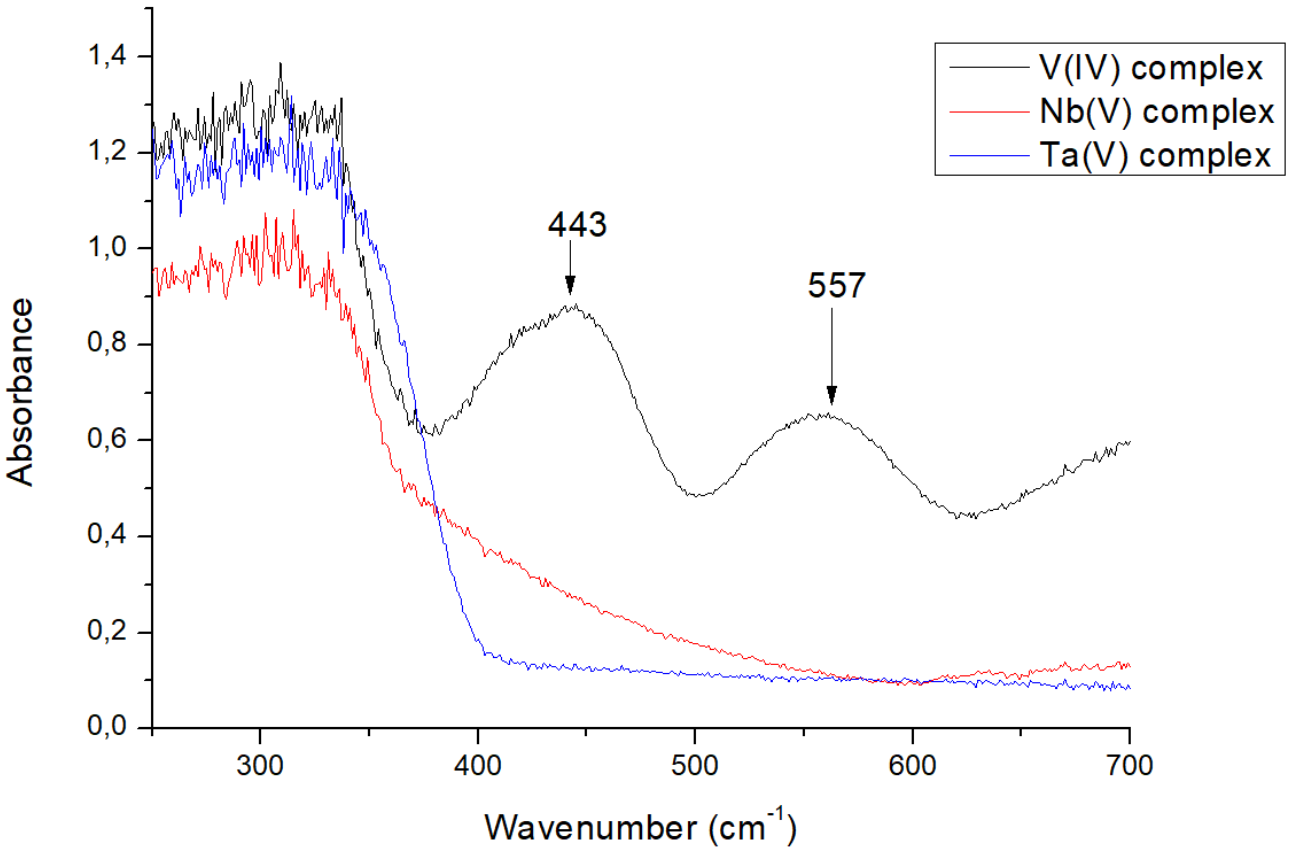

Figure S54. The UV-Vis diffuse reflectance spectra of V(IV), Nb(V) and Ta(V) complexes.

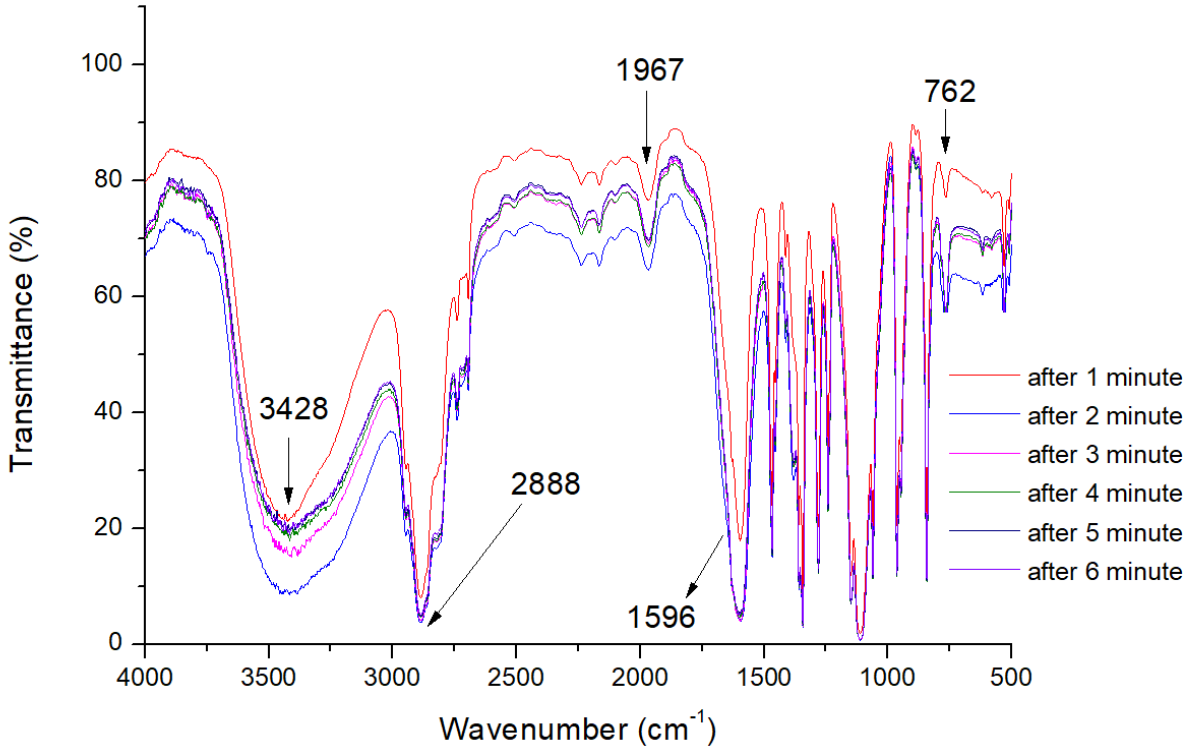

Figure S55. Time-resolved FTIR spectra of V-PE-50MMA during the self-healing process.

References

1 G. M. Sheldrick, *Acta Crystallogr A*, 2015, **71**, 3-8.

2 V. Petrícek, M. Dušek and L. Palatinus, *Zeitschrift für Kristallographie - Crystalline Materials,* 2014, **229**, 345-352.

3 M. C. Burla, R. Caliandro, B. Carrozzini, G. L. Cascarano, C. Cuocci, C. Giacovazzo, M. Mallamo, A. Mazzone and G. Polidori, *J Appl Crystallogr*, 2015, **48**, 306-309.

4 T. Gruene, H. W. Hahn, A. V. Luebben, F. Meilleur and G. M. Sheldrick, in *J. Appl. Crystallogr.*, 2014, **47,** 462-466.

5 O. V. Dolomanov, L. J. Bourhis, R. J. Gildea, J. A. K. Howard and H. Puschmann, *J. Appl. Crystallogr.*, 2009, **42**, 339-341.

6 A. H. Compton, *Nature,* 1915, **95**, 343–344.

7 C. F. MacRae, I. Sovago, S. J. Cottrell, P. T. A. Galek, P. McCabe, E. Pidcock, M. Platings, G. P. Shields, J. S. Stevens, M. Towler and P. A. Wood, *J Appl Crystallogr*, 2020, **53**, 226-235.

8 F. H. Allen, *Acta Crystallogr B*, 2002, **58**, 380-388.

9 M. J. Frisch, G. W. Trucks, H. B. Schlegel, G. E. Scuseria, M. A. Robb, J. R. Cheeseman, G. Scalmani, V. Barone, G. A. Petersson, H. Nakatsuji, X. Li, M. Caricato, A. V. Marenich, J. Bloino, B. G. Janesko, R. Gomperts, B. Mennucci, H. P. Hratchian, J. V. Ortiz, A. F. Izmaylov, J. L. Sonnenberg, D. Williams-Young, F. Ding, F. Lipparini, F. Egidi, J. Goings, B. Peng, A. Petrone, T. Henderson, D. Ranasinghe, V. G. Zakrzewski, J. Gao, N. Rega, G. Zheng, W. Liang, M. Hada, M. Ehara, K. Toyota, R. Fukuda, J. Hasegawa, M. Ishida, T. Nakajima, Y. Honda, O. Kitao, H. Nakai, T. Vreven, K. Throssell, J. A. Montgomery, Jr., J. E. Peralta, F. Ogliaro, M. J. Bearpark, J. J. Heyd, E. N. Brothers, K. N. Kudin, V. N. Staroverov, T. A. Keith, R. Kobayashi, J. Normand, K. Raghavachari, A. P. Rendell, J. C. Burant, S. S. Iyengar, J. Tomasi, M. Cossi, J. M. Millam, M. Klene, C. Adamo, R. Cammi, J. W. Ochterski, R. L. Martin, K. Morokuma, O. Farkas, J. B. Foresman, and D. J. Fox, Gaussian, Inc., Wallingford CT, 2016.

10 M. SudoŁ, K. Czaja and M. BiaŁek, *Polimery/Polymers*, 2000, **45**, 405-410.

11 G. Widmann and R. Riesen, *Anal Chim Acta*, 1982, **138**, 253-262.